DNMT3A Stability Is Maintained by Ubiquitin-Specific Peptidase 11 (USP11) and Sumoylation Countering Degradation

Taishi Yonezawa[1], Justine C. Rutter[2], Raghav Ramabadran[1], Venkatasubramaniam Sundaramurthy[1], Gandhar Datar[1], Mikolaj Slabicki[3], Margaret A. Goodell*[1]

1. Molecular and Cellular Biology Department; Stem Cells and Regenerative Medicine Center, Baylor College of Medicine, Houston, TX
2. Department of Medical Oncology, Dana-Farber Cancer Institute, Division of Hematology, Brigham and Women's Hospital, and Broad Institute of MIT and Harvard, Cambridge, MA
3. Krantz Family Center for Cancer Research, Massachusetts General Hospital Cancer Center, Boston, MA

* Correspondence: Margaret A. Goodell, goodell@bcm.edu

Abstract

DNA methyltransferase 3A (DNMT3A) plays crucial roles in hematopoiesis and mammalian development. DNMT3A protein instability has been associated with several diseases such as MDS, AML and Tatton-Brown-Rahman syndrome. Here we report, DNMT3A stability is maintained by deubiquitinating enzyme USP11 countering degradation by CUL4-DCAF8 E3 ligase. DNMT3A localization changes caused by certain unstable DNMT3A mutations, which could be considered one of the losses of function of DNMT3A. The mislocalization is partially rescued by E1 enzyme inhibition or stable USP11 expression lines. Interestingly, we show that USP11 enhances DNMT3A SUMOylation by promoting the interaction between DNMT3A and SUMO E3 Ligases, and DNMT3A SUMOylation also essential for maintaining DNMT3A protein stability and DNMT3A DNA Mtase activity. Our results reveal the mechanism for DNMT3A protein turnover through USP11, and the mechanism essential for DNMT3A function, as well as a therapeutic approach for several diseases causing DNMT3A protein instability.

Introduction

DNA methyltransferase 3A (DNMT3A) plays an important role in the regulation of hematopoietic stem cell (HSC) differentiation [1]. DNMT3A somatic mutations result in the clonal expansion of mutated hematopoietic stem cells (HSCs), a phenomenon called clonal hematopoiesis (CH). Many DNMT3A mutations have been identified in CH. CH accelerates with age and is associated with an ~11-fold increase in risk of hematologic disorders like myelodysplastic syndrome (MDS) and increased all-cause mortality [2, 3]. DNMT3A mutations have also been found to be associated with developmental growth disorders, such as Tatton-Brown-Rahman syndrome (TBRS). The symptoms of TBRS include intellectual disabilities, seizures, overgrowth, multiple developmental abnormalities, and a predisposition to cancer [4, 5]. Two major isoforms of DNMT3A exist: DNMT3A1 (full-length) and DNMT3A2 (short). DNMT3A1 is essential for neuronal gene expression and mouse postnatal development [6, 7]. Thus, DNMT3A is involved in hematopoiesis and development, and it is thought to be a tumor suppressor and developmental regulator.

Our recent study indicated that ~30% of CH-related DNMT3A mutations downregulate its expression at the protein level, and some of the DNMT3A mutations associated with CH overlap with its mutations in TBRS [8]. The DNMT3A R882 hotspot mutation accounts for approximately 60% of mutations in acute myeloid leukemia (AML), and the mutation has shown to act as a dominant negative [9-11]. The mutant protein does not differ significantly in protein expression compared to the DNMT3A WT. Importantly, in CH, the R882 mutation is found in only around 20% of cases. The proportion of DNMT3A unstable variants in CH is larger than that of the R882 mutation. Additionally, a previous report indicated that multivariate Cox regression showed that unstable DNMT3A mutants are an independent risk factor of AML even after accounting for age and gender. The hazard ratio of unstable DNMT3A mutants is higher than the R882 mutation. This indicates that unstable DNMT3A is strongly associated with CH and MDS risk [12]. For

DNMT3A related hematologic malignancies and TBRS, it is essential to understand unstable DNMT3A mutants at the molecular, animal, and clinical levels.

Using CRISPR screening [13], our recent study also revealed that the E3 ubiquitin ligase adaptor DCAF8 induced protein degradation in unstable (downregulated) DNMT3A mutants in 293T cells [8]. Additionally, this paper also found that DNMT3A WT is less susceptible to degradation by the ubiquitin system than DNMT3A unstable mutants. Based on these results, we hypothesize that DNMT3A WT has a molecular mechanism to keep its protein expression. Furthermore, understanding the mechanisms of DNMT3A protein turnover will be useful to develop a new therapeutic approach for hematologic malignancies and TBRS. However, the mechanisms of DNMT3A protein turnover remain incompletely understood; especially, which a deubiquitinating enzyme induces DNMT3A stabilization.

In this study, we repeated CRISPR screening using a neuroblastoma cell line whether our findings about DCAF8 are generalizable to other cell lines, animal models and clinical applications. Again, we identified DCAF8 as one of the DNMT3A degraders. We also found that Ubiquitin-Specific Peptidase 11 (USP11) induces DNMT3A deubiquitylation and stabilization countering degradation by DCAF8 from CRISPR screening and immunoprecipitation mass spectrometry (IP-Mass). We revealed that USP11 accelerates DNMT3A SUMOylation and the SUMOylation essential for DNMT3A protein stabilization. Furthermore, we revealed that USP11 maintains DNMT3A DNA methyltransferase (MTase) activity. Collectively, we found DNMT3A protein turnover maintained by the deubiquitinating enzyme USP11, and the SUMOylation of DNMT3A by inducing USP11 modulates DNMT3A DNA Mtase activity. The regulation of the activity of USP11 could be a new therapeutic strategy for CH and MDS caused by unstable DNMT3A.

Results

CRISPR screening identified DNMT3A protein modulators

The mechanism of DNMT3A protein turnover can be useful for developing new therapeutic approaches for hematologic malignancies and TBRS. However, the mechanisms of DNMT3A protein turnover remain poorly understood. First, we confirmed DNMT3A and DCAF8 protein and mRNA expression (Figure 1A and Supplementary Figure 1A) in several hematologic malignancy and neuroblastoma cell lines for repeating CRISPR Screening. Following mRNA expression level, DNMT3A and DCAF8 protein expressed in each cell line. In Kelly cells, both DNMT3A isoforms (DNMT3A1 and 2) and DCAF8 had higher protein expression levels. We evaluated the protein turnover of DNMT3A1 WT or unstable mutants (W297del and G685R) using ubiquitin-proteasome (UPS) inhibitors such as MG132 (proteasome inhibitor), TAK-243 (ubiquitin E1 enzyme inhibitor), and MLN4924 (neddylation inhibitor). Protein expression is highest in DNMT3A1 WT, followed by G685R, and lowest in W297del [8]. We generated 293T and Kelly cells, which are expressed DNMT3A1 WT or unstable mutants. The plasmid vector produces a DNMT3A1-GFP fusion protein, such that the level of GFP fluorescence allows us to infer the amount of DNMT3A1 protein present, and the fluorescence can be detected by flow cytometry. DsRed expression controls for transfection efficiency. Interestingly, the frequencies of protein turnover with UPS inhibitors were inversely proportional to the level of DNMT3A1 expression in the steady state, meaning that the UPS inhibitors had less dramatic effects on WT DNMT3A1 compared to W297del (Figure 1B-C). In both 293T and Kelly cells, these results were similar.

Since we observed a large change in the expression of the UPS inhibitor of $DNMT3A1^{W297Del}$, we repeated CRISPR screening to examine factors that mediate the stability of unstable mutant protein in Kelly cells. As in our previous study (293T cells), DCAF8 was enriched as a $DNMT3A1^{W297Del}$ degrader. We identified DCAF8 again as a $DNMT3A1^{W297Del}$ degrader in Kelly cells. We also identified several deubiquitinating enzymes (USP10, USP11 and USP41) as

potential stabilizers in the screening (Figure 1D-E and supplementary Figure 1B-C). As a result, these enzymes have a high potential for stabilizing DNMT3A.

The ubiquitin specific peptide USP11 induced DNMT3A deubiquitination and stabilization

Protein-protein interactions play a crucial role in protein turnover [14]. E3 ligases bind to target proteins and induce their ubiquitination and degradation. In contrast, deubiquitinating enzymes bind to substrate proteins and prevent ubiquitination and degradation. Therefore, it is imperative to determine which deubiquitinating enzymes can interact with DNMT3A for understanding DNMT3A protein turnover. Using IP-MS, we analyzed the interactome between DNMT3A1^{W297del} and deubiquitinating enzymes with or without the E1 ubiquitin inhibitor, which resulted in the stabilization of DNMT3A1^{W297del} (Figure2 A). Several deubiquitinating enzymes (USP1 and USP11) increased their interaction with DNMT3A1^{W297del} after DNMT3A1 ^{W297del} deubiquitylation (Figure 2B and supplementary Figure 2A-C). USP11 was identified as a stabilizer in both CRISPR and IP-MS screenings. These data indicate that DCAF8 plays a major role in degradation of DNMT3A1^{W297Del}, and USP11 is one of the strongest candidates for a major DNMT3A deubiquitinating enzyme (Figure 1E and Figure 2 B).

Following the results, we examined whether DCAF8 was involved in the interaction between DNMT3A1^{W297Del} and USP11. We introduced GFP-DNMT3A1^{W297Del} into 293T cells in the presence or absence of DCAF8. Cell lysates were subjected to IP with GFP trap [15], followed by immunoblotting with anti-USP11 to detect DNMT3A1^{W297Del} Interacted USP11. We found that USP11 strongly interacted with GFP-DNMT3A1^{W297Del} in DCAF8 KO 293T cells (figure 2C). Next, we examined whether USP11 induces DNMT3A1^{W297Del} deubiquitination. We introduced GFP-DNMT3A1^{W297Del} and Myc-USP11 into 293T cells. Cell lysates were subjected to IP with GFP trap, followed by immunoblotting with anti-ubiquitin to detect ubiquitinated DNMT3A1^{W297Del}. We identified that ubiquitinated DNMT3A1^{W297Del} was decreased by USP11 transduction into 293T cells(figure 2D). Finally, we investigated whether USP11 affects DNMT3A1^{W297Del} protein

expression in the presence or absence of DCAF8. USP11 overexpression increased DNMT3A1^{W297del} protein expression and the phenotype was boosted in DCAF8 KO 293T cells (Figure 2E-F). Taken together, USP11 is one of the DNMT3A deubiquitinating enzymes and maintains DNMT3A protein turnover countering DNMT3A ubiquitination and degradation by DCAF8.

The mislocalization of DNMT3A1 ^{W297del} was restored by inhibiting DNMT3A ubiquitination

DNMT3A has three functional domains, namely, Pro-Trp-Trp-Pro (PWWP), ATRX-DNMT3A-DNMT3L (ADD), and the methyltransferase (MTase) [16]. According to previous studies, several PWWP domain mutations, including W297del, are strongly associated with DNMT3A protein instability, and through these mutations, their localization from nucleus to cytoplasm is altered [17]. Next, we investigated whether DNMT3A1^{W297del} deubiquitination could restore DNMT3A1^{W297del} mislocalization. We generated 293T cells, which are expressed as DNMT3A1 WT or W297del mutant, and performed immunofluorescence analysis to confirm subcellular localization of DNMT3A1 WT and W297del mutant (Figure 3A-C and supplementary figure 3A-B). We extracted cytoplasmic, membrane, and nuclear proteins from the 293T cells which expressed DNMT3A1 WT or W297del mutant. We found that the mutant protein expression decreased in nucleus and increased cytoplasmic and membrane fraction (Figure 3D). Following the previous report, W297del mutant sequestered DNMT3A1 protein toward the cytoplasm, which resulted in a more diffuse localization pattern of DNMT3A1 in both the nucleus and cytoplasm.

We previously reported that DNMT3A1^{W297del} is strongly induced by ubiquitination and degradation by UPS, and inhibition of the E1 ubiquitin enzyme dramatically rescued and increased DNMT3A1^{W297del} protein expression. We hypothesized, not only DNM3A protein degradation, E1 ubiquitin enzyme also associates DNMT3A1 ^{W297del} mislocalization. We cultured DNMT3A1^{W297del} expressed 293T cells with TAK-243, an E1 inhibitor, and found that DNMT3A1 ^{W297del} localization was restored from cytoplasm to nucleus (Figure 3E supplementary figure 3C).

We confirmed whether deubiquitinating enzyme USP11 also related DNMT3A subcellular localization. We transduced USP11 into DNMT3A1^{W297del} expressed 293T cells. We found that endogenous USP11 is predominantly localized to the nucleus and nuclear membrane, while USP11 overexpression is localized to the nucleus and partly to the cytoplasm. Finally, we confirmed USP11 overexpression also modesty rescued DNMT3A^{W297del} mislocalization, which may relate USP11 subcellular localization (Figure 3F and supplementary figure 3D). Taken together we found that DNMT3A1^{W297del} mutant localization in the PWWP domain is regulated by the ubiquitin system, and blocking DNMT3A1^{W297del} ubiquitination restored its subcellular localization from the cytoplasm to the nucleus.

USP11 stimulates DNMT3A1 SUMOylation and facilitates its protein turnover

To further understand how the DNMT3A WT protein turnover is regulated, we examined the relationship between DNMT3A WT and USP11. First, we performed co-IP-MS to compare which proteins differentially interact with DNMT3A1 WT or W297del mutant (Figure 4A and Supplementary figure 4A-C). Interestingly, proteins involved in SUMOylation strongly and preferentially interacted with DNMT3A1 WT (Figure 4B). SUMOylation is one of the post-translational modifications that plays a role in protein stability, nuclear-cytosolic transport, and transcriptional regulation [18]. We also performed the co-IP-MS with W297del mutant in the presence or absence of DCAF8; W297del mutant preferentially interacted with SUMO proteins in DCAF8 KO cells (Figure 4C). Overall, we found that unstable DNMT3A loses its interaction with SUMO proteins, and we hypothesized that SUMOylation is important to DNMT3A stability and turnover.

We then examined whether USP11 is involved in DNMT3A1 SUMOylation. We treasured FLAG-DNMT3A1, Myc-USP11 and HA-SUMO3 into 293T cells. Cell lysates were subjected to IP with FLAG (DNMT3A1) antibody, followed by immunoblotting with anti-HA (SUMO3) to detect DNMT3A SUMOylation (Figure 4D). Additionally, we try to detect endogenous DNMT3A

SUMOylation. We treasured FLAG-DNMT3A1, Myc-USP11 into 293T cells and Cell lysates were subjected to immunoprecipitation with FLAG (DNMT3A1), followed by immunoblotting with anti-SUMO3 to detect endogenous DNMT3A1 SUMOylation (Figure 4E). We confirmed that USP11 induced DNMT3A1 SUMOylation in the endogenous level, and our findings suggest that DNMT3A1 protein stability and SUMOylation are maintained by UPS11. We then looked at the inhibition of SUMOylation associated with DNMT3A protein turnover. We cultured Kelly (neuroblastoma) and THP-1 (hematologic malignancy) cell lines with TAK-981, a first-in-class Inhibitor of SUMO-Activating Enzyme [19] (Figure 4F). We confirmed that TAK-981 strongly reduced protein expression of DNMT3A1 but not DNMT3A2 (short isoform and lack of N-terminus) (Figure 4G, H). We also performed co-IP to compare USP11 interaction with DNMT3A1 or DNMT3A2. We transduced Myc-USP11 and FLAG-DNMT3A1 or DNMT3A2 into 293T cells. Cell lysates were subjected to IP with FLAG (DNMT3A1 or 2) antibody, followed by immunoblotting with anti-Myc (USP11) to detect the interaction between USP11 and DNMT3A1 or 2. Interestingly, USP11 strongly interacted with DNMT3A1. The N-terminus of DNMT3A may be helpful for DNMT3A and USP11 interaction (Supplementary Figure 4A-C). We also confirmed whether endogenous USP11 protein expression is involved in DNMT3A protein expression in Kelly cells. We transduced Cas9 protein and USP11 targeted sgRNA into Kelly cells and followed by WB. The depletion of USP11 decreased DNMT3A1 protein expression (Supplementary Figure 4D-F).

As a result, DNMT3A prefers to interact with SUMO proteins for its stabilization. Protein SUMOylation is essential for SUMO E3 ligase interaction with target proteins [20]. We then examined whether USP11 enhances DNMT3A1-SUMO E3 ligase interaction. We treasured GFP-DNMT3A1, and Myc-USP11 into 293T cells. Cell lysates were subjected to immunoprecipitation with GFP trap, and we performed MS analysis (Figure 5A). We confirmed that USP11 promotes the binding of multiple E3 SUMO ligases (CBX4 and PIAS1) to DNMT3A1 (Figure 5B). These SUMO E3 ligases may accelerate DNMT3A1 SUMOylation and protein turnover.

Taken together, USP11 promoted deubiquitination and SUMOylation of DNMT3A1 and maintained its protein turnover.

DNA Mtase activity of DNMT3A was enhanced by USP11

Finally, we examined whether USP11 is involved in the methyltransferase activity on DNMT3A1 using the HOXA5-Snrpn-blue fluorescence (BFP) reporter system [21, 22]. In 293T cells, we inserted a Snrpn-blue fluorescence protein (BFP) reporter into the HOXA5 promoter locus, so that increased DNA methylation at HOXA5-Snrpn-BFP would lead to decreased BFP levels (Figure 5C). Through this strategy, methyltransferase functionality can be readout by flow cytometry. To test the fidelity of the assay, we transduced the cells with a retrovirus vector carrying HA-USP11 (co-expressing puromycin resistant gene). Puromycin was used to create stable USP11 expression strains, and then we transduced the cells with a retrovirus vector carrying DNMT3A1(co-expressing GFP). Following the introduction of DNMT3A1, the percentage of BFP-positive cells declined predominantly. USP11 alone slightly reduced BFP-positive cells less than DNMT3A alone. On the other hand, co-expression of DNMT3A1 and USP11 dramatically reduced BFP expression (Figure 5D-F). Based on these findings, we found that USP11 strongly increases DNA Mtase activity of DNMT3A1 in the HOXA5 prompter region.

Discussion

The work presented here, characterizing the mechanisms of DNMT3A protein turnover. Our previous report indicated that DNMT3A variants associated with CH and TBRS patients have revealed general principles of DNMT3A regulation and stability, which can be used to interpret novel variants throughout a wide variety of diseases. This work also revealed that DNMT3A destruction by the $CUL4B^{DCAF8}$ E3 ligase illustrates a new biological pathway, which may lead to new potential therapeutic approaches to CH and TBRS. However, the mechanisms of DNMT3A protein turnover remain incompletely understood; particularly why WT DNMT3A can retain expression. Furthermore, it is not known which deubiquitinating enzymes can remove DNMT3A ubiquitination and degradation by DCAF8.

Using CRISPR screening and IP-Mass, we identified several deubiquitinating enzymes (USP1, USP10, USP11 and USP41), which potentially induces DNMT3A deubiquitinating and stabilization. Interestingly, a previous report indicated that DCAF8 and USP11 regulate myeloid leukemia factors (MLFs) in opposite directions [23]. The CRISPR screening identified DCAF8 as a degrader of DNMT3A, consistent with our previous findings. We also identified USP11 as a candidate of DNMT3A stabilizer countering DCAF8. Therefore, USP11 and DCAF8 play opposite roles in DNMT3A protein turnover. However, it is unclear why USP11 and DACF8 are specifically involved in the regulation of proteolysis. There is a need for a deeper understanding of their molecular mechanisms. Furthermore, we identified other E3 ligases and deubiquitinating enzymes such as RNF26, USP1, USP10 and USP41. It may also be possible that these ubiquitin regulators are involved in the protein turnover of DNMT3A, so further investigation is needed.

We identified DNMT3A SUMOylation was induced by USP11 and USP11 enhanced the interaction between DNMT3A and E3 SUMO ligases such as CBX4 and PIAS1. Previous reports indicated that SUMOylation enhanced DNMT1 DNA MTase activity [24], and SUMOylation also enhances DNMT family DNA binding efficiency [25]. Protein-DNA binding is important to protein stabilization [26]. USP11 may accelerate DNA binding of DNMT3A through SUMOylation and it

may lead to DNMT3A protein stabilization and deubiquitination. Moreover, previous research suggests that PIAS1 knockout mice exhibit abnormal differentiation of hematopoietic stem cells caused by Dnmt3a DNA MTase deficiency [27]. These results imply DNMT3A SUMOylation essential for its protein function. We also found that DNMT3A DNA MTase activity accelerated by USP11 in the cell-based assay. It would be very useful to investigate the relationship between DNMT3A and USP11 using animal models in the future.

A recent study showed that DNMT3A is normally recruited to intergenic regions by H3K36me2, but DNMT3A^{W297Del} unstable mutant failed to bind to chromatin [28]. Nuclear receptor binding SET domain protein (NSD) 1 and 2 are essential for H3K36 demethylation [29] , and another study indicated that the deubiquitination of H2AK119ub and H3K36 demethylation by inducing NSD2-proteasome 26S subunit, non-ATPase 14 (PSMD14) [30]. H2AK119ub is also regulated by DNMT3A and USP11 [7, 31, 32], but it remains unclear how these proteins relate to the modification of H2AK119ub, and it may be related to the relation of H3K36me2 and DNMT3A with its protein stability. It is necessary to investigate the relationship between DNM3A protein turnover and histone modification further.

In many CH-related DNMT3A mutations, the protein expression is downregulated, and some CH-related DNMT3A mutations overlap with TBRS mutations. It has been suggested that DNMT3A mutations causing protein instability may lead to the development of MDS, AML, and TBRS. In terms of therapeutic potential, DNMT3A protein regulation is a good target. We showed that TAK-243, an E1 enzyme, inhibitor and USP11 could restore DNMT3A protein expression and mislocalization. These data suggested that DNMT3A deubiquitination has a potential to be a strategy to modulate DNMT3A protein turnover. In mice models, TAK-243 has shown therapeutic effects in several human cancer xenograft models [33], and future research should examine TAK-243's therapeutic effects and side effects on unstable DNMT3A *in vivo*. The inhibition of DCAF8 is also a therapeutic target. Therefore, the development of DCAF8 inhibitors may be useful and Dcaf8 KO mice need to be used to confirm the phenotype and side effects. We may not avoid

several side effects, if we use TAK-243 and a DCAF8 inhibitor, because TAK-243 and DCAF8 have multiple targets in the cells. The development of DNMT3A-targeted Deubiquitinase-targeting chimeras (DUBTACs) is another solution. DUBTACs directory induce protein interaction between a target protein and a deubiquitinating enzyme [34]. As a result, the target protein is induced by deubiquitination and protein stabilization by the deubiquitinating enzyme. Meanwhile, Proteolysis Targeting Chimeras (PROTACs) induce interaction between a target protein and an E3 ligase, resulting in ubiquitination and degradation [35]. Because it degrades the target protein directly, there are fewer side effects. Another advantage of PROTACs and DUBTACs is that they can regulate the protein turnover of target proteins, which is not limited to endogenous target protein degradation mechanisms. Other than the DNMT3A ^{W297del} mutant, unstable DNMT3A mutants can likely be regulated even if they are regulated for degradation by proteins other than USP11 and DCAF8; DNMT3A targeted DUBTACs are likely to be effective in treating 30% of DNMT3A variant for CH treatment and prevention. We have already discovered that USP11 is one of the deubiquitinating enzymes of DNMT3A in this study. USP11 also increased DNMT3A DNA MTase activity. Therefore, creating DNMT3A-USP11 specific DUBTAC could be an effective treatment for DNMT3A instability-related CH and diseases such as MDS, AML and TBRS.

Finally, in this study we have shown that new molecular mechanisms DNMT3A protein turnover by USP11. Through modulating DNMT3A function, USP11 may play a significant role in HSC regulation and neural development. We also are confident that our findings will be useful in the prevention and treatment of unstable DNMT3A mutation-related diseases.

Methods

Cell culture

Kelly, THP-1, Loucy, P31, Fuji SR706 and U937 cells were cultured in RPMI-1640 with 10% fetal bovine serum (FBS) and 1% penicillin-streptomycin. 293T, D425, NH12 and Onda9 cells were cultured in DMEM with 10% fetal bovine serum (FBS) and 1% penicillin-streptomycin.

Plasmids

For DNMT3A expression, FLAG-tagged DNMT3A1 or 2 in a pCAG vector and GFP-tagged DNMT3A1 in a pLenti vector were used. For Myc-tagged USP11 and HA-tagged SUMO3 in a pCDNA3 vector were used for their expression. FLAG-tagged DNMT3A1 in a pMYs-IRES-GFP (pMYs-IG) vector were used to express DNMT3A1, and HA-tagged USP11 in a pMYs-IRES-Puro vector were used to express USP11.

CRISPR-DNMT3A Stability Screen

The human BISON CRISPR-KO library, which contains 2,852 guide RNAs, targets 713 E1, E2, E3, deubiquitinases, and control genes [13]. It was cloned into the pXPR003 as previously described [36] by the genome perturbation platform (Broad Institute). The lentivirus particles for the library were produced in a T-175 flask format. Briefly, 18 °ø 106 Kelly cells were seeded in 25 mL DMEM supplemented with 10% FBS and penicillin/streptomycin/glutamine. The next day, a packaging mix was prepared: 40 µg psPAX2, 4 µg pVSV-G, and 32 µg of the library in 1 mL OptiMem (Invitrogen) and incubated for 5 minutes at room temperature. This mix was combined with 244 µL TransIT-LT1 (Mirus) in 5 mL OptiMem, incubated for 30 minutes at room temperature, and then applied to cells. Two days post transfection, cell debris was removed by centrifugation. The lentivirus particles containing medium were collected and stored at −80°C before use. Kelly cells were engineered with constitutively expressing Cas9 and bicistronic DNMT3AW297Del reporter. Then, 2 °ø 106 engineered 293T cells were added with 10% (v/v) of the human BISON CRISPR-KO in 2 mL medium and spin-infected (2,400 rpm, 2 hours, 37°ΔC). Twenty-four hours post infection, sgRNA-infected cells were selected with 2 µg/mL puromycin for 2 days. On the

ninth day postinfection, populations were separated using fluorescence activated cell sorting. Two populations were collected (top 5% and lowest 5%) based on the eGFPDNMT3A to mCherry MFI ratio. Sorted cells were harvested by centrifugation and subjected to direct lysis buffer reactions (1 mmol/L CaCl2, 3 mmol/L MgCl2, 1 mmol/L EDTA, 1% Triton X-100, Tris pH 7.5, with freshly supplemented 0.2 mg/mL proteinase). The sgRNA sequence was amplified in a first PCR reaction with eight staggered forward primers. Then, 20 µL of direct lysed cells was mixed with 0.04 U Titanium Taq (Takara Bio 639210), 0.5 °ø Titanium Taq buffer, 800 µmol/L dNTP mix, 200 nmol/L P5-SBS3 forward primer, and 200 nmol/L SBS12-pXPR003 reverse primer in a 50-µL reaction. The samples were heat activated at 94°∆C for 5 minutes; kept at 94°∆C for 30 seconds, 58°∆C for 10 seconds, and 72°∆C for 30 seconds and repeated from the second step for 15 cycles; and heated at 72°∆C for 2 minutes. Then, 2 µL of the primary PCR product was used as the template for 15 cycles of the secondary PCR, where Illumina adapters and barcodes were added [0.04 U Titanium Taq (Takara Bio 639210), 1 °ø Titanium Taq buffer, 800 µmol/L dNTP mix, 200 nmol/L SBS3-Stagger-pXPR003 forward primer, 200 nmol/L P7-barcode-SBS12 reverse primer]. An equal amount of all samples was pooled and subjected to preparative agarose electrophoresis followed by gel purification (Qiagen). Eluted DNA was further purified by NaOAc and isopropanol precipitation. Amplified sgRNAs were quantified using the Illumina NextSeq platform. Read counts for all guides targeting the same gene were used to generate P values. The data analysis pipeline comprised the following steps: (i) Each sample was normalized to the total read number. (ii) For each guide, the ratio of reads in the stable versus unstable sorted gate was calculated, and guide RNAs were ranked. (iii) The ranks for each guide were summed for all replicates. (iv) The gene rank was determined as the median rank of the four guides targeting it. (v) P values were calculated, simulating a corresponding distribution over 100 iterations.

Transfection, western blotting, and immunoprecipitation

293T cells were transiently transfected with 5 ug of vector, GFP or FLAG-tagged DNMT3A, MYC-tagged USP11, or HA-tagged SUMO3 mixed with lipofectamine 2000. The cells were cultured for 48 h after the transfection and lysed in Hypotonic buffer and Lysis buffer (see below). For FLAG-targeted immunoprecipitation, the cell lysates were incubated with anti-FLAG M2 (SIGMA, Louis, MO, USA, Catalog Number F3165) antibody for 15 min at 25°C. Then the samples were incubated with Dynabeads protein-G (Thermo Fisher Scientific, Waltham, MA, USA) for 15 min at 25°C. For GFP-targeted immunoprecipitation the cell lysates were incubated GFP trap (Protein Tek GFP-Trap® Magnetic Agarose, IL, USA, Catalog Number gtma-20) for 60 min at 4°C The precipitates were washed three times with cell lysis buffer (Cell Signaling Technology, Danvers, MA, USA, Catalog Number 9803) containing 1 mM phenylmethanesulfonylfluoride fluoride, subjected to sodium dodecyl sulfate-polyacrylamide gel electrophoresis (SDS-PAGE), and analyzed by western blotting. For some experiments, we isolated nuclear and cytoplasmic fractions before the immunoprecipitation (see below). Western blotting was performed with anti-FLAG M2-Peroxidase (Sigma, Catalog Number A8592), anti-Myc 9E10 (Santa Cruz Biotechnology, sc-40), anti-HA-Peroxidase (Roche, 12CA5), anti-GFP (NOVUS, Catalog Number NB600-308), anti-USP11 (Abcom, Catalog Number ab109232), anti-Lamin B1 (Santa Cruz Biotechnology, Catalog Number B1304), anti-GAPDH (Cell Signaling Technology, Catalog Number 5174), anti-AIF (Cell Signaling Technology, Catalog Number 5318), Anti-DCAF8 Bethyl lab, Catalog Number A301-556A), anti-B-actin (Cell Signaling Technology, Catalog Number, 3700S), and anti-SUMO2/3 (Cell Signaling Technology, Catalog Number, 4971). Signals were detected by using Clarity Western ECL Substrate (BioRad, Catalog Number, 170-5060), and immunoreactive bands were visualized using a ChemiDoc MP imaging System (BioRad,Catalog Number 12003154). Band intensities were measured using ImageLab (BioRad).

Immunofluorescence analysis

293T cells introduced with control vector, GFP-tagged DNMT3A, which is coexpressed DsRed were fixed with 2% paraformaldehyde, permeabilized with 0.2% Triton X-100, blocked with 2%

BSA, and then incubated with anti-GFP (NOVUS, Catalog Number NB600-308) and anti-USP11 (Abcom, Catalog Number ab109232) antibodies, followed by labeling with Alexa Fluor 568–conjugated anti-rabbit antibody (Thermo Fisher Scientific, Catalog Number A11011) and Alexa Fluor 488–conjugated anti-mouse antibody (Thermo Fisher Scientific, Catalog Number A11034). Nuclei were visualized with DAPI (Bio Legend). Fluorescent images were analyzed on a Keyence BZ-X800 microscope (Keyence).

Viral transduction

Retroviruses for human cells and lentiviruses were produced by transient transfection of 293T cells with viral plasmids along with gag-, pol-, and env-expressing plasmids using the calcium-phosphate method [37]. Retrovirus transduction to the cells was performed using Retronectin (Takara Bio Inc., Otsu, Shiga, Japan).

IP Mass spectrometry

The cells were lysed in 3 volumes of NETN buffer (50mM Tris pH 7.3, 170mM NaCl, 1mM EDTA, 0.5% NP-40) using probe sonication followed by ultracentrifugation at 44,000rpm for 20min at 4oC. The lysate was incubated with 20µl of GFP-Trap agarose beads (Chromotek gta) for 1hr at 4oC. The beads were briefly washed with lysis buffer, boiled in 2X NUPAGE® LDS sample buffer (Invitrogen) and subjected to SDS-PAGE (NuPAGE 10% Bis-Tris Gel, Invitrogen). In-gel protein digestion of whole lane was done using trypsin and LysC protease mix. The LC-MS/MS analysis was carried out using a nanoLC1000 system coupled to Orbitrap Fusion mass spectrometer (Thermo Scientific, San Jose, CA). The MS raw data was searched in Proteome Discoverer 2.1 software (Thermo Scientific, San Jose, CA) with Mascot algorithm (v2.4, Matrix Science) against the human NCBI refseq database (updated 2021_12_23). The peptides identified from mascot result file were validated with 5% false discover rate (FDR). The gene product inference and quantification were done with label-free iBAQ approach using ‘gpGrouper’ algorithm [PMID: 30093420]. The differentially expressed proteins were calculated using the moderated t-test to calculate p-values and log2 fold changes in the R package limma [PMID: 25605792]. For

statistical assessment, missing value imputation was employed through sampling a normal distribution N(μ-1.8 σ, 0.8σ), where μ, σ are the mean and standard deviation of the quantified values.

HOXA5-Snrpn-BFP Methylation Reporter Analysis

HOXA5-Snrpn-BFP Methylation Reporter Analysis DNA for the Snrpn promoter, BFP (tagBFP), woodchuck hepatitis virus post translational regulatory elements, bovine growth hormone polyadenylation signal, and HOXA5 homology arms were synthesized (Genscript). The linearized targeting vector was cotransfected with sgRNA-HOXA5 and Cas9-expressing vectors in 293T cells. 100,000 HOXA5- Snrpn-BFP cells were seeded to 6 well-plates and then mixed with DNMT3A or/and USP11 lentiviral particles in three biological replicates.

UPS11 depletion using the CRISPR/Cas9 system

Targeting human USP11, 1ug sgRNA (Synthego) (UCUGGGCCCCAGGUUCCUUG for gRNA-1, GCUUCUCCACAAGGAACCUG for gRNA-2), was incubated with 1 μg Cas9 protein (PNA Bio) for 30 minutes at room temperature to obtain Cas9-sgRNA RNPs. Next, the RNPs and 2×10^5 Kelly cells were mixed and electroporated using the optimized electroporation condition of 1,200 V, 20 ms, and two pulses by Neon transfection system (Thermo FisherScientific).

Figure 1

Targeted CRISPR screening identifies E3 ligases and deubiquitinating enzymes essential for DNMT3A protein turnover.

A, The image depicts DNMT3A and DCAF8 protein expression followed by western blotting using DNMT3A, DCAF8 and GAPDH antibodies.

B, The image depicts the scheme of ubiquitin-proteasome inhibitor assay for confirming DNMT3A protein turnover changes.

C, The graph depicts the protein expression of DNMT3A WT and unstable mutants (W297del and G685R) with ubiquitin-proteasome inhibitors. Alterations in DNMT3A protein stability after administration of proteasome inhibitor (MG132), a CRL inhibitor (MLN4924), an E1 and ubiquitin enzyme inhibitor (TAK-243) Stability ratio of MFI of DNMT3A-GFP versus MFI of mCherry before and after treatment with the ubiquitin-proteasome inhibitors as measured by flow cytometry 48 hours after transfection.

D, Schematic of targeted CRISPR screening to identify ubiquitin modulators essential for DNMT3A protein turnover. Kelly cells were engineered to constitutively overexpress Cas9 and the indicated bicistronic DNMT3A^{W297Del} reporter and then infected with sgRNA libraries targeting ubiquitin ligases. Nine days after infection, we sorted both the top and bottom 5% of cells for DNMT3A-GFP expression.

E, the graph depicts the gene enrichment score and P value in targeted CRISPR screening for ubiquitin modulators. DCAF8, USP20, and USP28 genes (red) and USP10, USP11 and USP41 (blue) were enriched and statistically significant.

Figure 2

USP11 regulated DNMT3A protein turnover countering protein degradation by FCAF8

A, Schematic of immunoprecipitation (IP) mass spectrometry to identify deubiquitinating enzymes essential to interact with DNMT3A. Kelly cells were engineered to constitutively overexpress the indicated bicistronic GFP-DNMT3A^{W297Del} reporter and treated with TAK-243. To subjects cell lysate was performed I P and mass spectrometry analysis.

B, The graph depicts the enriched score of the interaction between DNMT3A^{W297del} and deubiquitinating enzymes with or without 1nM TAK-243 for 6 hours.

C. 293T cells were transfected with GFP-DNMT3A1^{W297Del}. Cell lysates were immunoprecipitated with anti-GFP antibody, following the detection of USP11-bound DNMT3A1^{W297Del} with anti-USP11 antibody.

D. 293T cells were transfected with GFP-DNMT3A1^{W297Del}. Cell lysates were immunoprecipitated with anti-GFP antibody, following the detection of DNMT3A1^{W297Del} ubiquitination with anti-ubiquitin antibody.

E, F. In the presence or absence of DCAF8, 293T cells were transfected with GFP-DNMT3A1^{W297Del} and/or Myc-USP11. Cell lysates were immunoblotted following the detection of DNMT3A1^{W297Del}, USP11 and DCAF8 protein expression with anti-GFP -Myc and -DCAF8 antibodies. F; The graph depicts the protein expression in Figure 2E

Figure 3

DNMTA deubiquitination restored the mislocalization of DNMT3A^{W297del}

A, B 293T cells were transfected with GFP- DNMT3A WT or -W297del and were stained anti-USP11 (rabbit) antibodies followed by anti-rabbit Alexa 647 (yellow). DNMT3A expression detected GFP (Green), nuclei and cytoplasm detached, DsRed (Red). Nuclei were visualized with DAPI (Blue). Laser scanning microscopy (Keyence) was used for the imaging.

C, The graph depicts the subcellular localization pattern of GFP- DNMT3A WT or -W297del.

D, 293T cells were transfected with GFP-DNMT3A WT or -W297del. nuclear, membrane/organelle and cytoplasmic fractions were isolated, following the detection of DNMT3A with anti-GFP antibody. GAPDH was used as a loading control for cytoplasm, AIF for membrane/organelle, and LAMIN-B for nuclear proteins.

E, 293T cells were transfected with GFP-DNMT3A1^{W297del} and were stained anti-USP11 (rabbit) antibodies followed by anti-rabbit Alexa 647 (yellow) with or without 1nM of TAK-243 for 6 hours. DNMT3A expression detected GFP (Green), nuclei and cytoplasm detached, DsRed (Red). Nuclei were visualized with DAPI (Blue). Laser scanning microscopy (Keyence) was used for the imaging. The graph depicts the subcellular localization pattern of GFP-W297del with or without TAK-243.

F, 293T cells were transfected with GFP-W297del and USP11 were stained anti-USP11 (rabbit) antibodies followed by anti-rabbit Alexa 647 (yellow), DNMT3A expression detected GFP (Green), nuclei and cytoplasm detected DsRed (Red), nuclei were visualized with DAPI (Blue). Laser scanning microscopy (Keyence) was used for the imaging. The graph depicts the subcellular localization pattern of GFP-W297del with or without USP11 overexpression.

Figure 4

USP11 induced DNMT3A SUMOylation and its essential for DNMT3A protein stability

A, Schematic of immunoprecipitation (IP) mass spectrometry to identify comparing DNMT3A stable (DNMT3A WT or W297Del in the absence of DCAF8) or an unstable protein (W297Del) interactome. 293T cells were engineered to constitutively overexpress the indicated bicistronic GFP-DNMT3A WT or W297Del reporter in the presence or absence of DCAF8. To subjects cell lysate was performed I P and mass spectrometry analysis.

B, C, The graph depicts the enriched score of the interaction proteins with stable DNMT3A or unstable DNMT3A.

D, 293T cells were transfected with FLAG-DNMT3A1, Myc-USP11 and HA-SUMO3. Cell lysates were immunoprecipitated with anti-FLAG (DNMT3A) antibody, following the detection of DNMT3A1 SUMOylation with anti-HA antibody.

E, 293T cells were transfected with FLAG-DNMT3A1, Myc-USP11. Cell lysates were immunoprecipitated with anti-FLAG (DNMT3A) antibody, following the detection of DNMT3A1 endogenous SUMOylation with anti-SUMO2/3 antibody.

F. The scheme depicts TAK-981, a first-in-class Inhibitor of SUMO-Activating enzymes.

G,H, Kelly or THP- cells were cultured with 1uM ofTAK-981 for 24 hours. Cell lysates were detected with anti-DNMT3A, -SUMO2/3 and -B-actin antibodies.

Figure 5

USP11 induced DNMT3A SUMOylation and its essential for DNMT3A protein stability

A, Schematic of immunoprecipitation (IP) mass spectrometry to identify DNMT3A E3 SUMO ligases. 293T cells were engineered to constitutively overexpress the indicated bicistronic GFP-DNMT3A WT reporter and transduced Myc-USP11. To subjects cell lysate was performed I P and mass spectrometry analysis.

B, The graph depicts the interacted SUMO related proteins with DNMT3A1.

C, The graph depicted DNMT3A DNA Methyltransferase activity analysis using the HOXA5-Snrpn-BFP methylation. Knocking in (KI) Snrpn promoters to the HOXA5 locus in reverse orientation in 293T cells linked to BFP and bovine polyA signals.

D, E, Methyltransferase activity assay. The figure depicts blue fluorescence intensity in the FLAG-DNMT3A and/or HA-USP11 transduced cells as measured by flow cytometry on day 10. The graphs depicted the BFP positive cells. The negative control frequency of BFP+ cells was set as 1. One-way ANOVA with Tukey's multiple comparisons was completed. *$p < 0.05$, **$p < 0.01$ *** $p < 0.001$ ****$p < 0.0001$.

F, A representative western blot of 293T cells expressing HOXA5-Snrpn-BFP, FLAG-DNMT3A1 and or HA-USP11.

Supplemental Figure 1

A, The image depicts DNMT3A and DCAF8 mRNA expression in the DepMap (https://depmap.org/portal/)

B, The graph depicts the gene enrichment score for DCAF8, USP11 in the CIRSPR screening.

C, The graph depicts the read counts for DCAF8, USP11 in the CRISPR screening.

Supplemental Figure 2

A, The images show representative SDS-PAGE for the DNMT3A IP-mass.

B, The graph depicts the protein expression of DNMT3A and deubiquitinating enzymes on IP-mass with DNMT3A. with or without 1nM TAK-243 for 6 hours.

C, B, The graph depicts the enriched score of the interaction between DNMT3A^{W297del} and DNMT3A interacted proteins with or without 1nM TAK-243 for 6 hours.

Supplemental Figure 3

A-D 293T cells were transfected with GFP- DNMT3A WT or -W297del with or without 1nM TAK-243 for 6 hours or USP11 overexpression. We stained anti-USP11 (rabbit) antibodies followed by anti-rabbit Alexa 647 (yellow). DNMT3A expression detected GFP (Green), nuclei and cytoplasm detached, DsRed (Red). Nuclei were visualized with DAPI (Blue). Laser scanning microscopy (Keyence) was used for the imaging.

Supplemental Figure 4

A, The images show representative SDS-PAGE for the DNMT3A IP-mass.

B, C, The graph depicts the protein expression of DNMT3A or DCAF8 on IP-mass with DNMT3A.

Supplemental Figure 5

A, 293T cells were transfected with FLAG-DNMT3A1 or 2 and Myc-USP11. Cell lysates were immunoprecipitated with anti-FLAG (DNMT3A) antibody, following the detection of DNMT3A interacted USP11 with anti-myc antibody for western blotting.

B, C, The graph depicts the protein expression of DNMT3A in input control or IP in the supplemental figure 5A.

D, Kelly cells were transduced with a vector control or two independent gRNAs targeting USP11. The gRNAs showed efficient depletion of USP11. The image depicts DNMT3A, USP11 and B-action protein expression followed by western blotting using DNMT3A, USP11and B-actin antibodies.

E, F, The graph depicts the protein expression of USP11, DNMT3A1 and 2 in the supplemental figure 5D.

Supplemental Figure 6

A, B, The figure depicts blue fluorescence intensity in the FLAG-DNMT3A and/or HA-USP11 transduced cells as measured by flow cytometry on day 10. The graphs depicted the BFP positive cells.

Author contributions

T. Y. designed and performed experiments, analyzed the data, and wrote the paper. R. R., V. S., and G. D. assisted with experiments. M. S., and J. R. performed the CRISPR screening. P. G. conceived the project, designed experiments, analyzed the data, and wrote the paper.

Acknowledgments

We thank the Flow Cytometry Core, the Mass Spectrometry Proteomics Core and the Genetically Engineered Rodent Models Core at Baylor College of Medicine. This work was supported by NIH NCI R01 CA183252 (PG), NIDDK R01 DK092883 (PG), NCI 1P01CA265748-01 (PG), Leukemia & Lymphoma Society Career Development Program (TY), Cancer Research Institute Irvington Postdoctoral Fellow (TY), Japan Society for the Promotion Science Research Fellow (TY), TOYOBO Biotechnology Foundation (TY) and Yamada Science Foundation (TY). I appreciate Dr. Margaret Goodell laboratory members and collaborators.

References

Reference list

1. Challen, G.A., et al., *Dnmt3a is essential for hematopoietic stem cell differentiation.* Nat Genet, 2011. **44**(1): p. 23-31.
2. Xie, M., et al., *Age-related mutations associated with clonal hematopoietic expansion and malignancies.* Nat Med, 2014. **20**(12): p. 1472-8.
3. Genovese, G., et al., *Clonal hematopoiesis and blood-cancer risk inferred from blood DNA sequence.* N Engl J Med, 2014. **371**(26): p. 2477-87.
4. Tatton-Brown, K., et al., *Mutations in the DNA methyltransferase gene DNMT3A cause an overgrowth syndrome with intellectual disability.* Nat Genet, 2014. **46**(4): p. 385-8.
5. Tatton-Brown, K., et al., *The Tatton-Brown-Rahman Syndrome: A clinical study of 55 individuals with de novo constitutive DNMT3A variants.* Wellcome Open Res, 2018. **3**: p. 46.
6. Chen, T., et al., *A novel Dnmt3a isoform produced from an alternative promoter localizes to euchromatin and its expression correlates with active de novo methylation.* J Biol Chem, 2002. **277**(41): p. 38746-54.
7. Gu, T., et al., *The disordered N-terminal domain of DNMT3A recognizes H2AK119ub and is required for postnatal development.* Nat Genet, 2022. **54**(5): p. 625-636.
8. Huang, Y.H., et al., *Systematic Profiling of DNMT3A Variants Reveals Protein Instability Mediated by the DCAF8 E3 Ubiquitin Ligase Adaptor.* Cancer Discov, 2022. **12**(1): p. 220-235.
9. Kim, S.J., et al., *A DNMT3A mutation common in AML exhibits dominant-negative effects in murine ES cells.* Blood, 2013. **122**(25): p. 4086-9.
10. Russler-Germain, D.A., et al., *The R882H DNMT3A mutation associated with AML dominantly inhibits wild-type DNMT3A by blocking its ability to form active tetramers.* Cancer Cell, 2014. **25**(4): p. 442-54.
11. Holz-Schietinger, C., D.M. Matje, and N.O. Reich, *Mutations in DNA methyltransferase (DNMT3A) observed in acute myeloid leukemia patients disrupt processive methylation.* J Biol Chem, 2012. **287**(37): p. 30941-51.
12. Dohoon Lee, et al., *AMLs harboring DNMT3A-destabilizing variants show increased intratumor DNA methylation heterogeneity at bivalent chromatin domains.* BioRxiv, 2023.
13. Slabicki, M., et al., *The CDK inhibitor CR8 acts as a molecular glue degrader that depletes cyclin K.* Nature, 2020. **585**(7824): p. 293-297.

14. Welchman, R.L., C. Gordon, and R.J. Mayer, *Ubiquitin and ubiquitin-like proteins as multifunctional signals.* Nat Rev Mol Cell Biol, 2005. **6**(8): p. 599-609.
15. Yilmazer, I., et al., *Determining Protein-Protein Interaction with GFP-Trap Beads.* Methods Mol Biol, 2023. **2564**: p. 317-323.
16. Yang, L., R. Rau, and M.A. Goodell, *DNMT3A in haematological malignancies.* Nat Rev Cancer, 2015. **15**(3): p. 152-65.
17. Christian, D.L., et al., *DNMT3A Haploinsufficiency Results in Behavioral Deficits and Global Epigenomic Dysregulation Shared across Neurodevelopmental Disorders.* Cell Rep, 2020. **33**(8): p. 108416.
18. Vertegaal, A.C.O., *Signalling mechanisms and cellular functions of SUMO.* Nat Rev Mol Cell Biol, 2022. **23**(11): p. 715-731.
19. Langston, S.P., et al., *Discovery of TAK-981, a First-in-Class Inhibitor of SUMO-Activating Enzyme for the Treatment of Cancer.* J Med Chem, 2021. **64**(5): p. 2501-2520.
20. Hendriks, I.A. and A.C. Vertegaal, *A comprehensive compilation of SUMO proteomics.* Nat Rev Mol Cell Biol, 2016. **17**(9): p. 581-95.
21. Huang, Y.H., et al., *DNA epigenome editing using CRISPR-Cas SunTag-directed DNMT3A.* Genome Biol, 2017. **18**(1): p. 176.
22. Stelzer, Y., et al., *Tracing dynamic changes of DNA methylation at single-cell resolution.* Cell, 2015. **163**(1): p. 218-29.
23. Huang, D., et al., *CRL4(DCAF8) and USP11 oppositely regulate the stability of myeloid leukemia factors (MLFs).* Biochem Biophys Res Commun, 2020. **529**(2): p. 127-132.
24. Lee, B. and M.T. Muller, *SUMOylation enhances DNA methyltransferase 1 activity.* Biochem J, 2009. **421**(3): p. 449-61.
25. Borgermann, N., et al., *SUMOylation promotes protective responses to DNA-protein crosslinks.* EMBO J, 2019. **38**(8).
26. Andrabi, M., K. Mizuguchi, and S. Ahmad, *Conformational changes in DNA-binding proteins: relationships with precomplex features and contributions to specificity and stability.* Proteins, 2014. **82**(5): p. 841-57.
27. Liu, B., et al., *PIAS1 SUMO ligase regulates the self-renewal and differentiation of hematopoietic stem cells.* EMBO J, 2014. **33**(2): p. 101-13.
28. Weinberg, D.N., et al., *The histone mark H3K36me2 recruits DNMT3A and shapes the intergenic DNA methylation landscape.* Nature, 2019. **573**(7773): p. 281-286.

29. Lucio-Eterovic, A.K., et al., *Role for the nuclear receptor-binding SET domain protein 1 (NSD1) methyltransferase in coordinating lysine 36 methylation at histone 3 with RNA polymerase II function.* Proc Natl Acad Sci U S A, 2010. **107**(39): p. 16952-7.
30. He, L., et al., *The proteasome component PSMD14 drives myelomagenesis through a histone deubiquitinase activity.* Mol Cell, 2023. **83**(22): p. 4000-4016 e6.
31. Chen, X., et al., *Structural basis for the H2AK119ub1-specific DNMT3A-nucleosome interaction.* Nat Commun, 2024. **15**(1): p. 6217.
32. Ting, X., et al., *USP11 acts as a histone deubiquitinase functioning in chromatin reorganization during DNA repair.* Nucleic Acids Res, 2019. **47**(18): p. 9721-9740.
33. Hyer, M.L., et al., *A small-molecule inhibitor of the ubiquitin activating enzyme for cancer treatment.* Nat Med, 2018. **24**(2): p. 186-193.
34. Henning, N.J., et al., *Deubiquitinase-targeting chimeras for targeted protein stabilization.* Nat Chem Biol, 2022. **18**(4): p. 412-421.
35. Bekes, M., D.R. Langley, and C.M. Crews, *PROTAC targeted protein degraders: the past is prologue.* Nat Rev Drug Discov, 2022. **21**(3): p. 181-200.
36. Doench, J.G., et al., *Optimized sgRNA design to maximize activity and minimize off-target effects of CRISPR-Cas9.* Nat Biotechnol, 2016. **34**(2): p. 184-191.
37. Yonezawa, T., et al., *The ubiquitin ligase STUB1 regulates stability and activity of RUNX1 and RUNX1-RUNX1T1.* J Biol Chem, 2017. **292**(30): p. 12528-12541.

Figure1

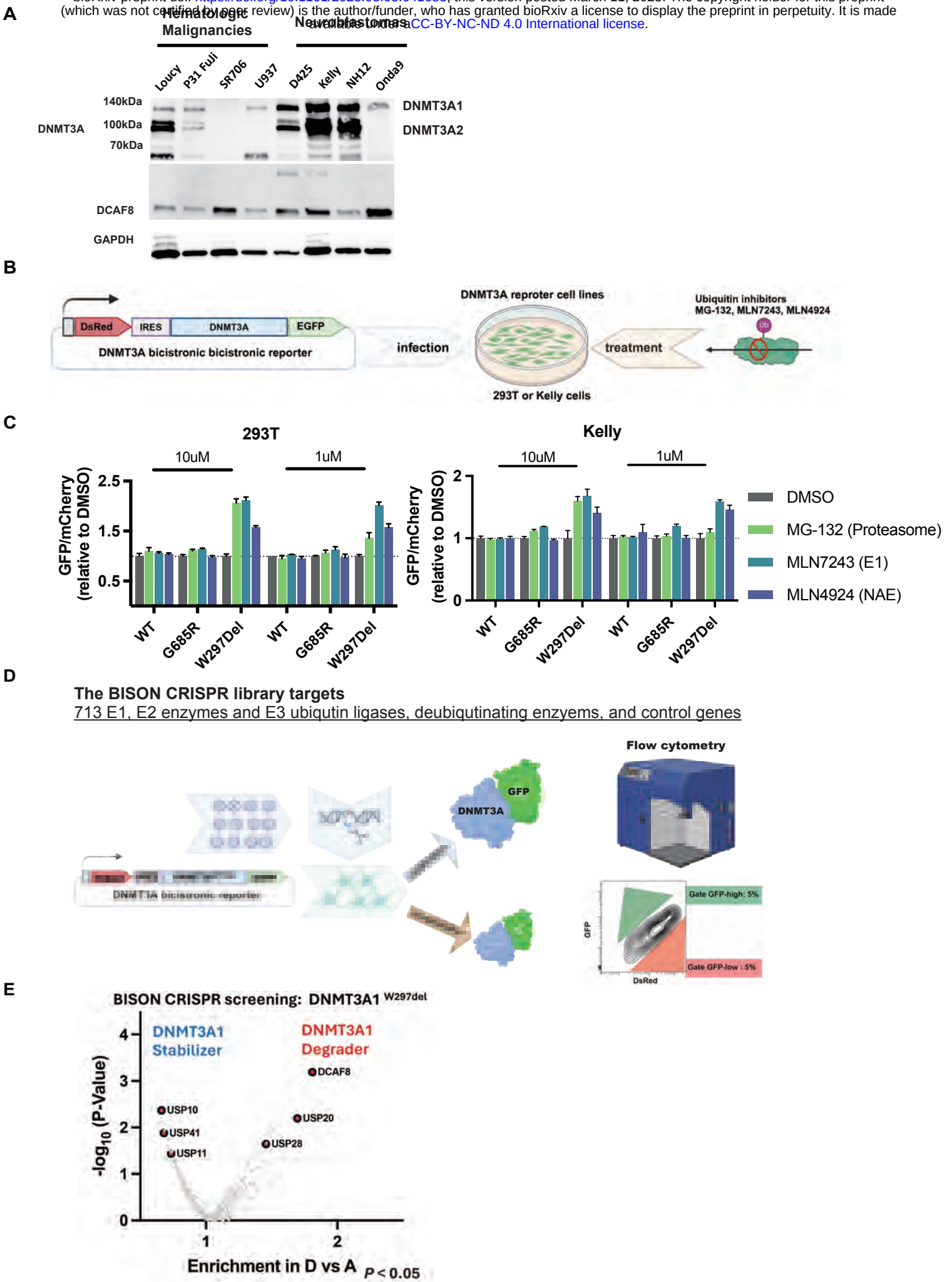

Figure2

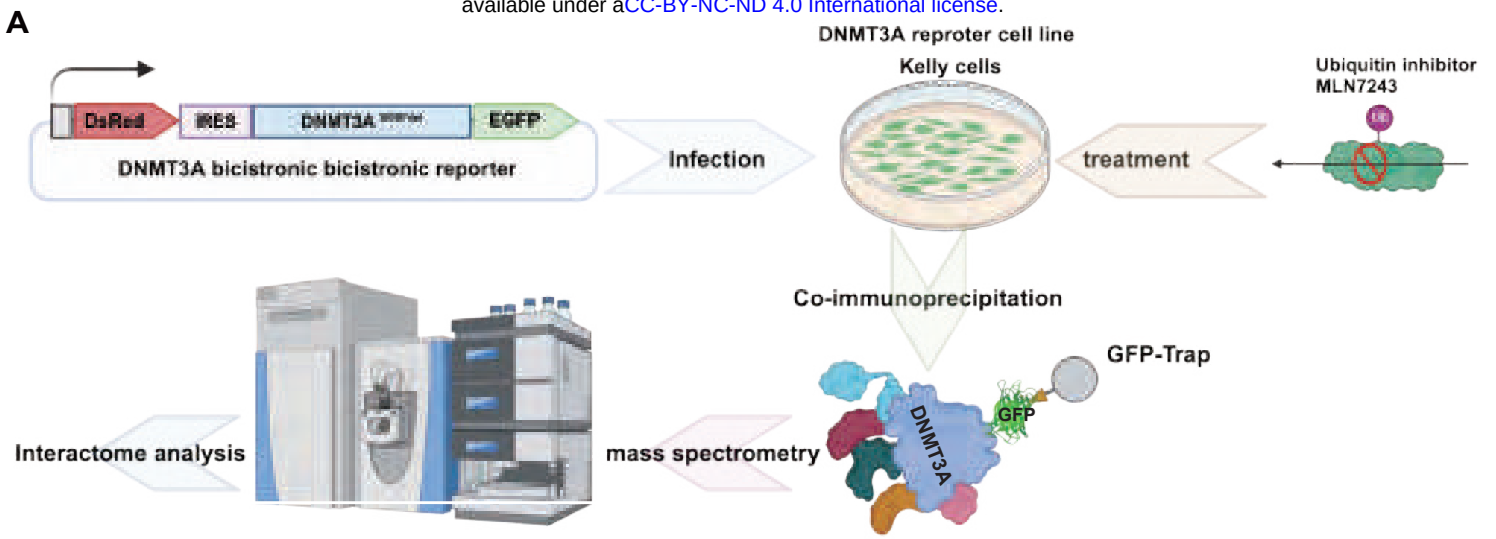

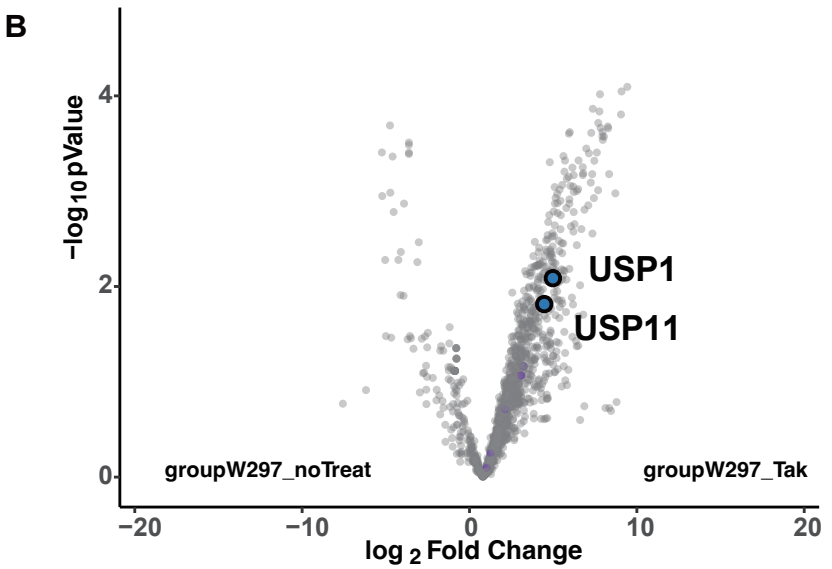

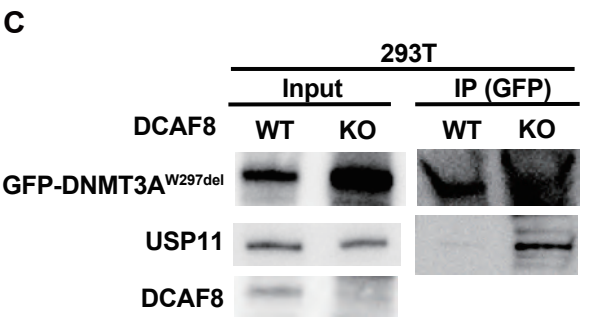

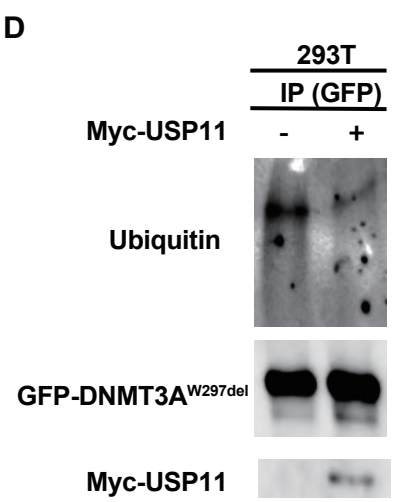

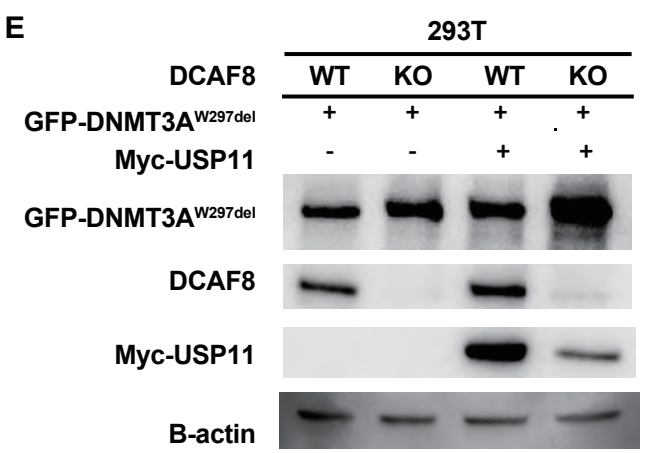

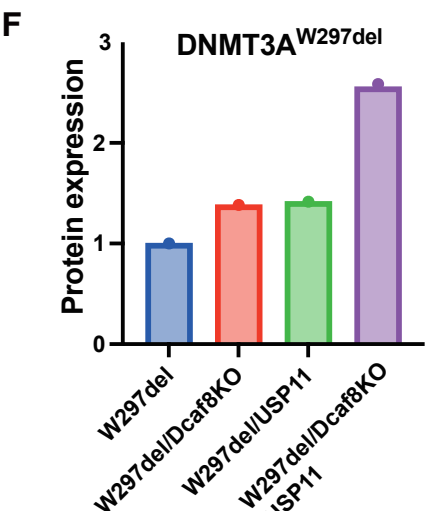

Figure3

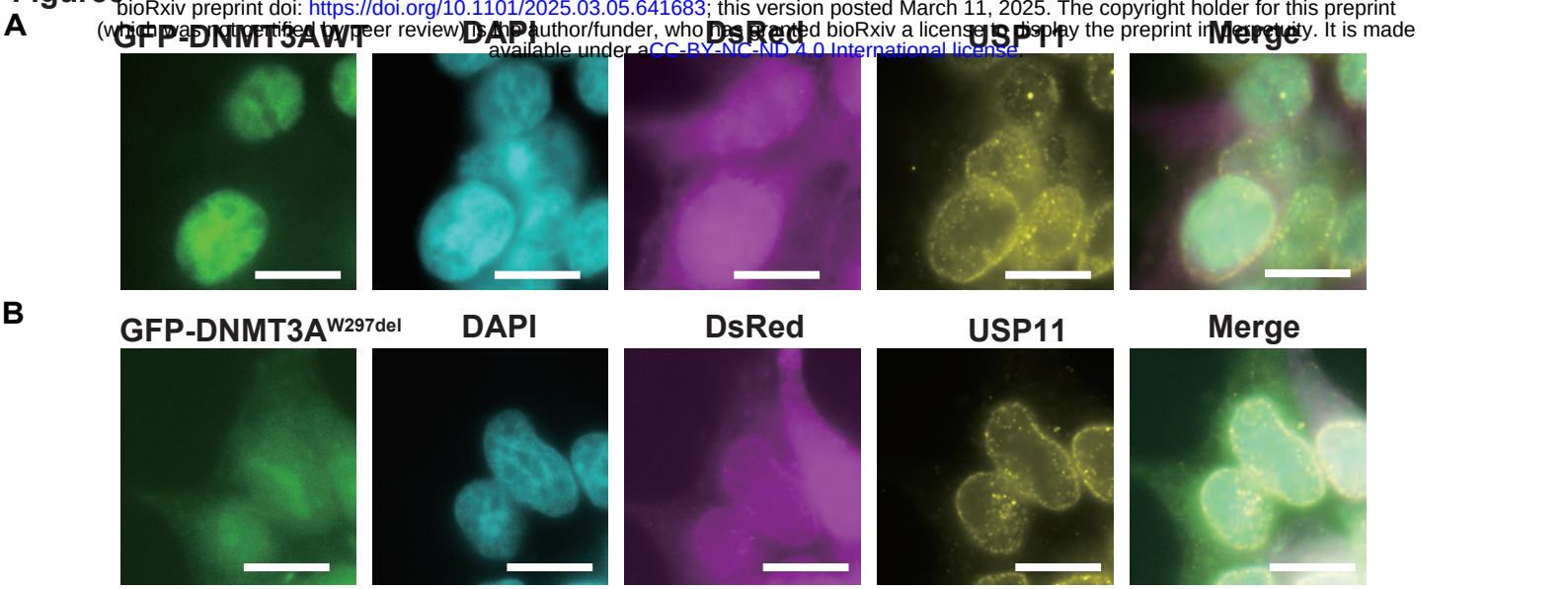

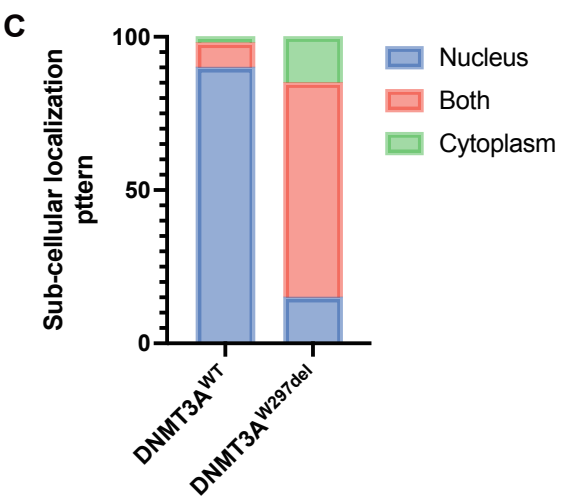

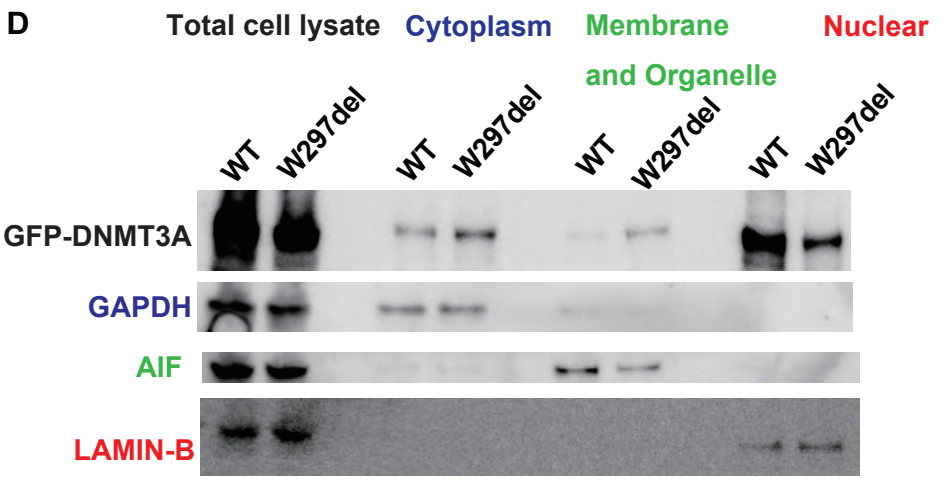

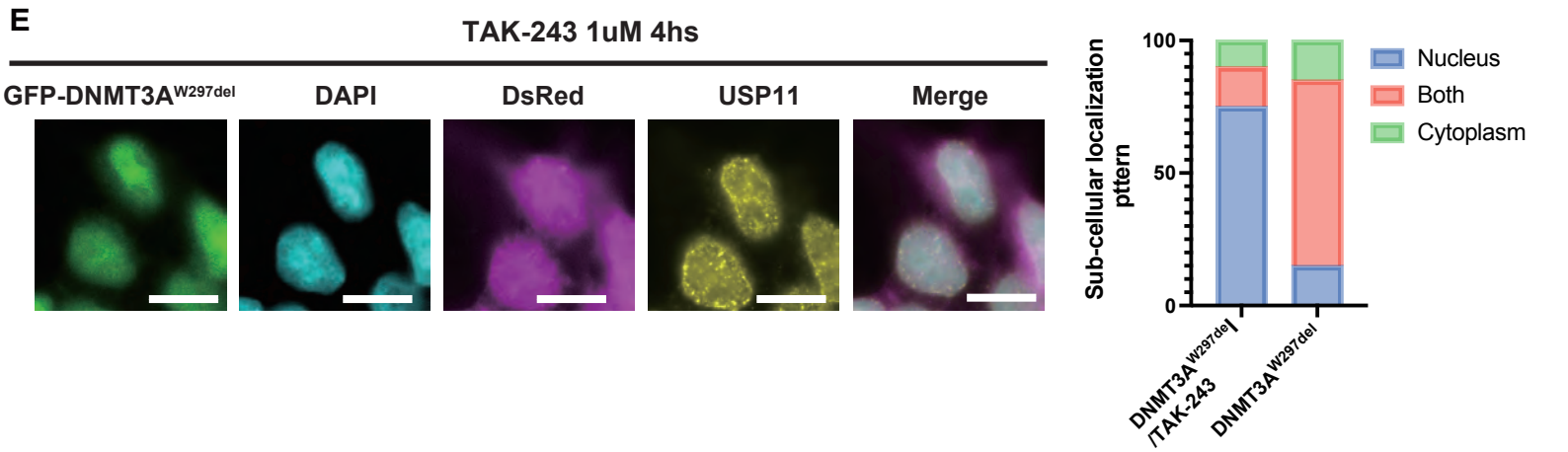

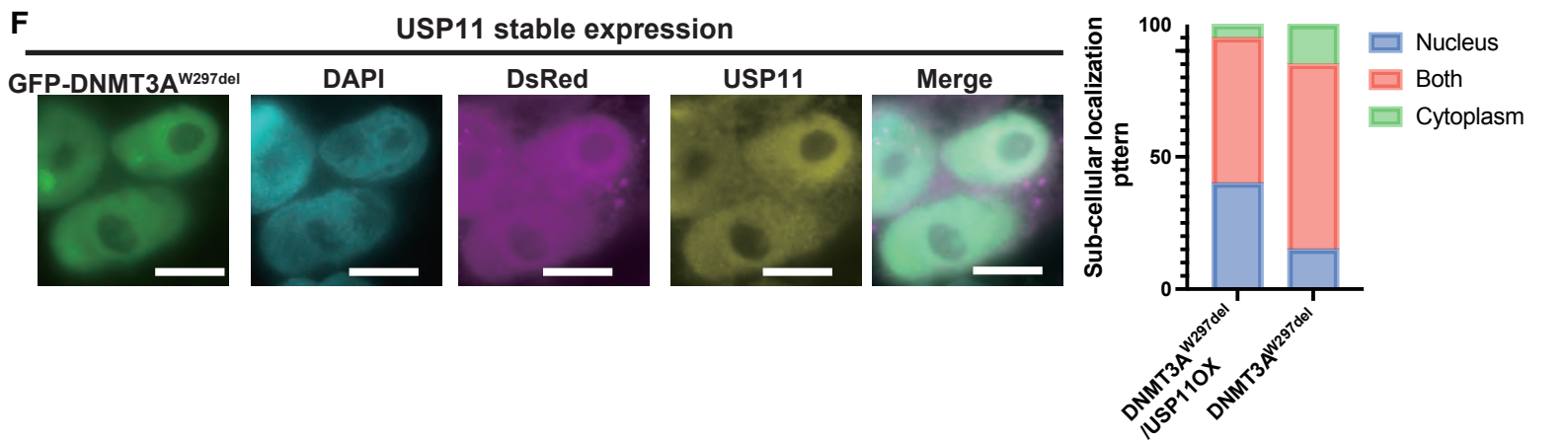

Figure4

A

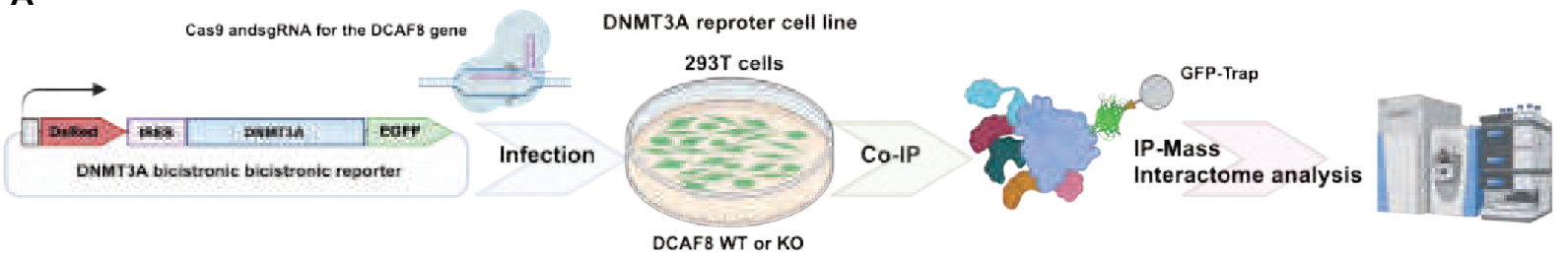

B

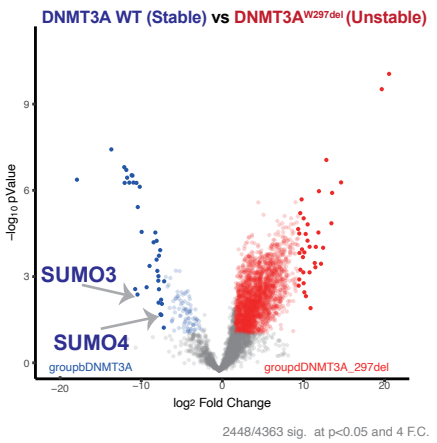

C

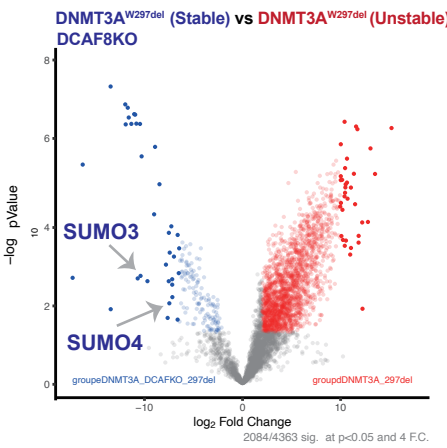

D

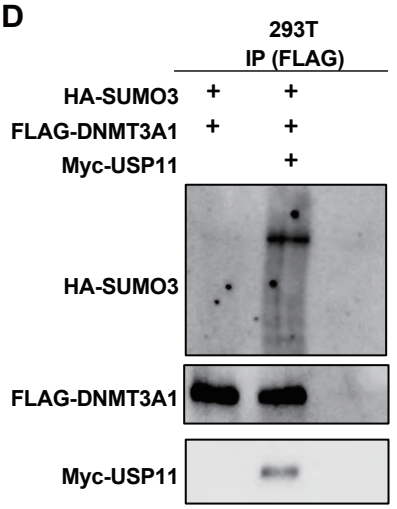

E

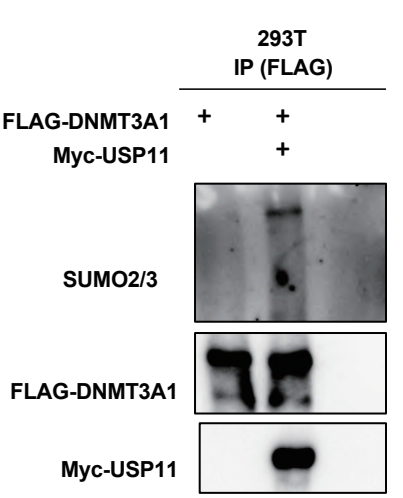

F

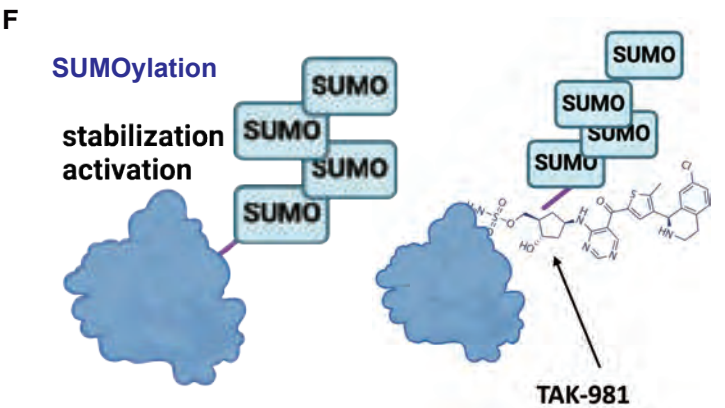

G

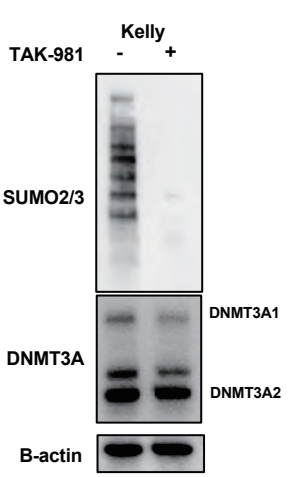

H

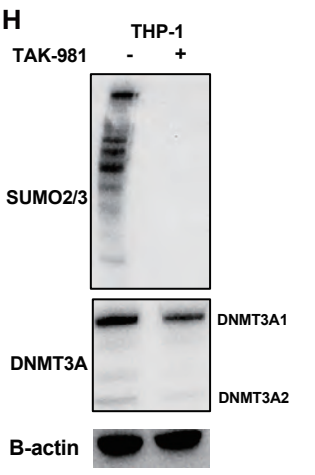

Figure5

A

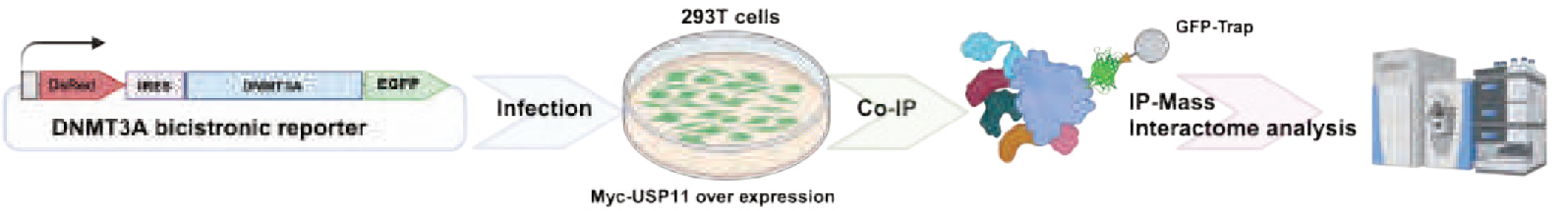

B

Accession	Description	Coverage	# PSMs	# Peptides
4885649	SUMO-activating enzyme subunit 2 [Homo sapiens]	26.71875	45	15
55770830	E3 SUMO-protein ligase CBX4 [Homo sapiens]	21.7857143	23	11
767985566	E3 SUMO-protein ligase PIAS1 isoform X1 [Homo sapiens]	7.57575758	7	4

C

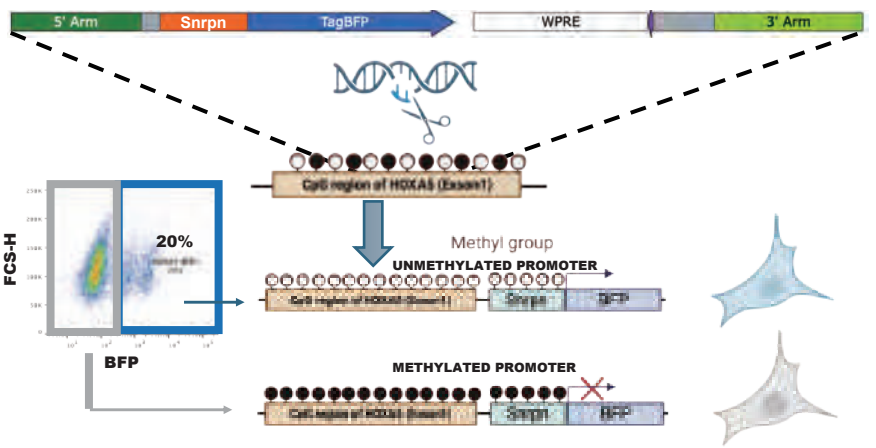

D

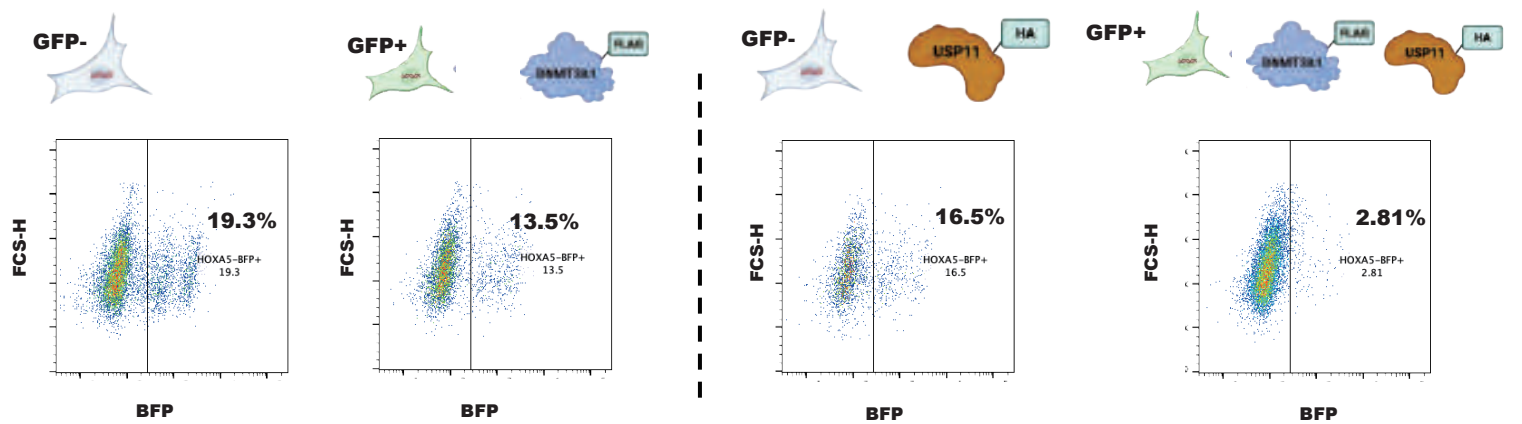

E

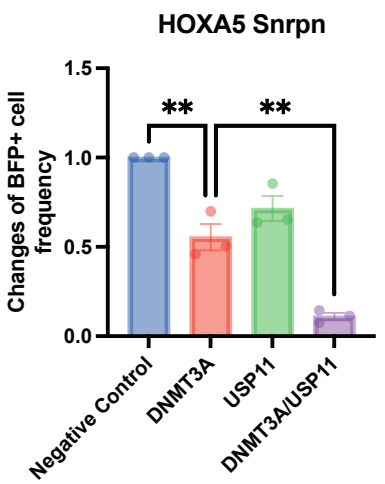

F

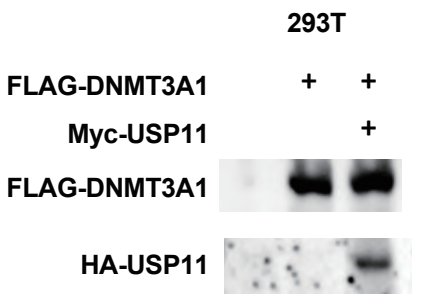

A

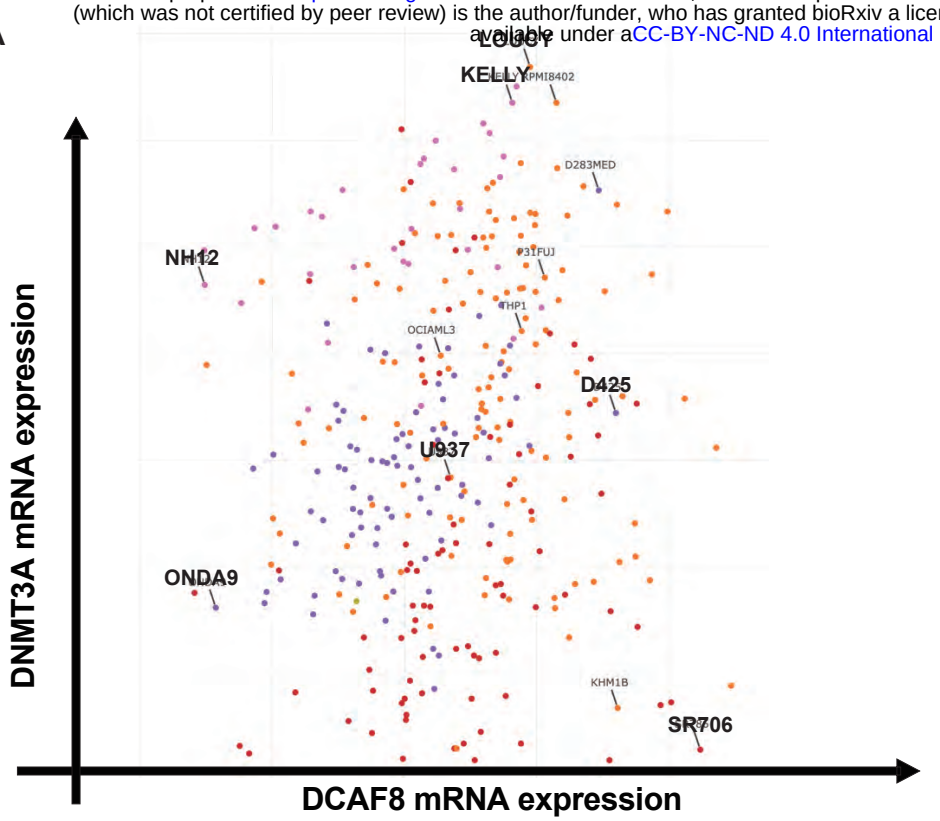

B

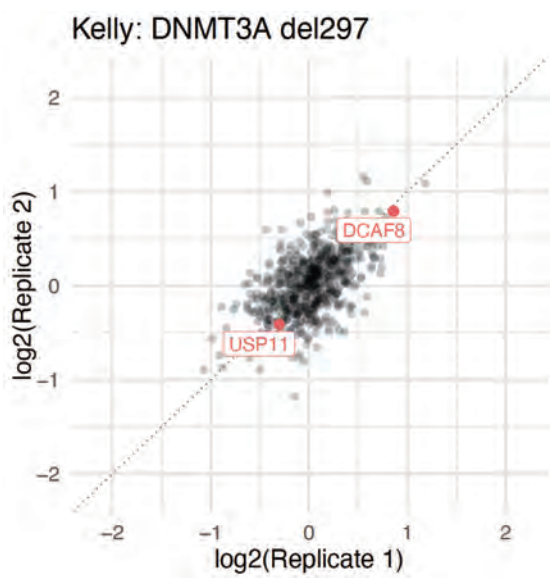

C

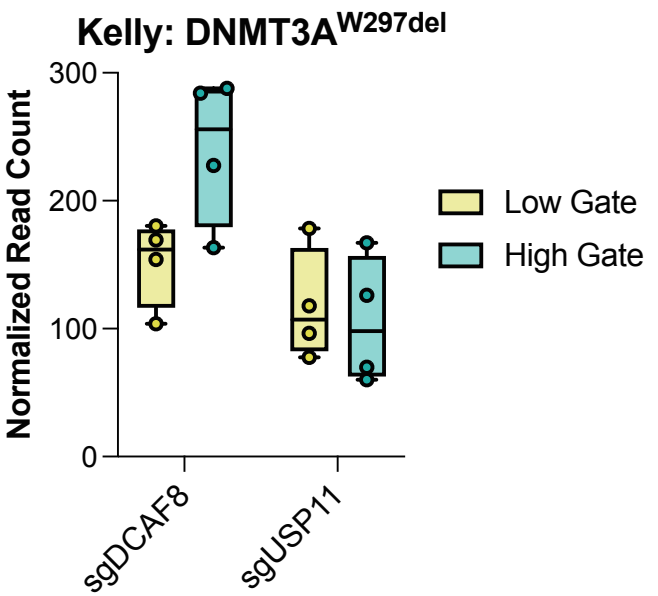

A

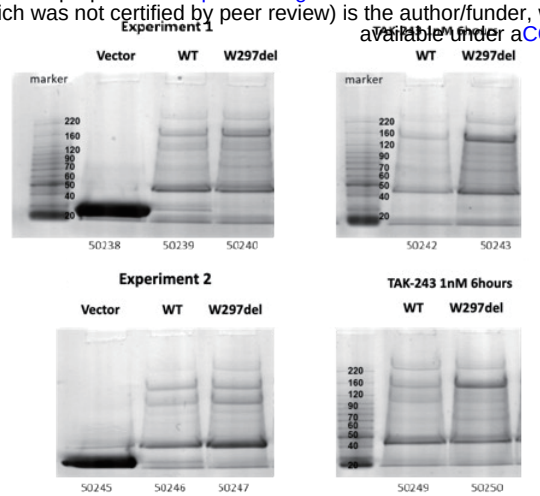

B

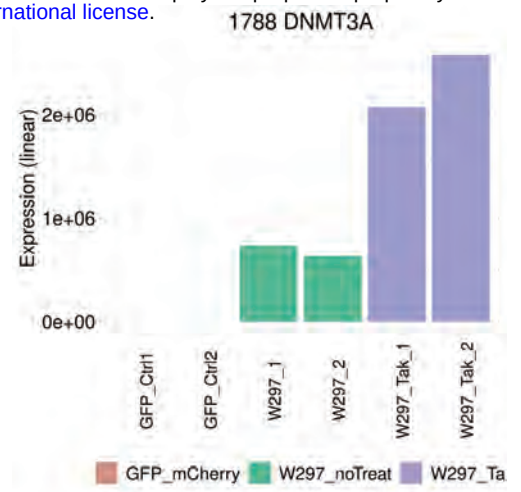

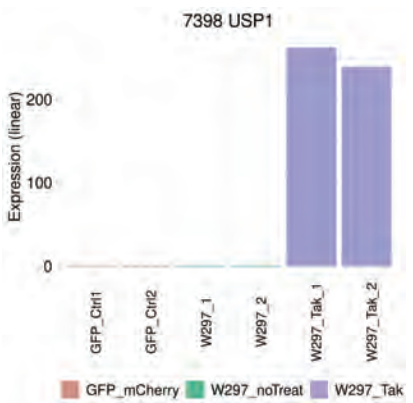

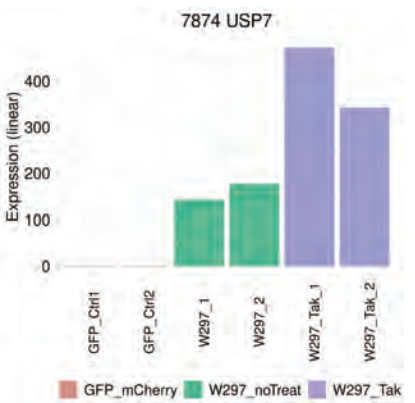

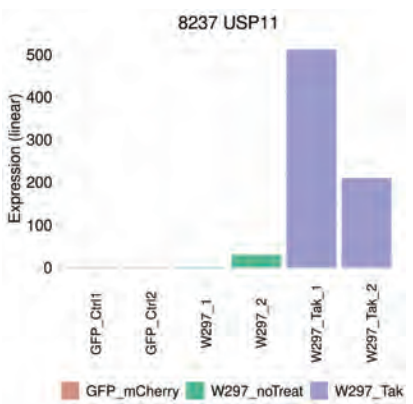

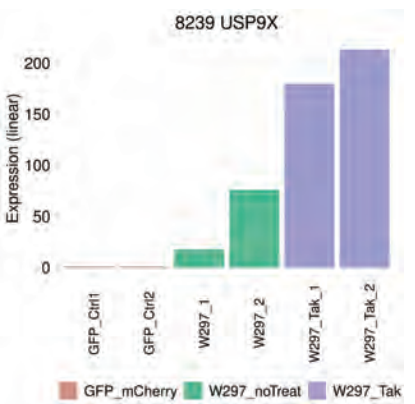

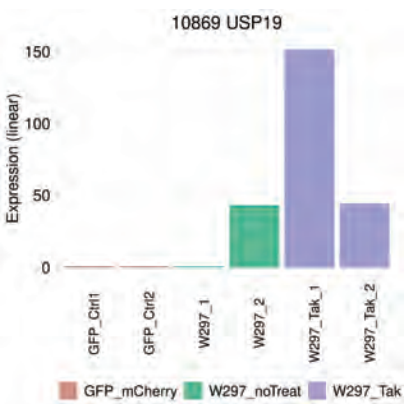

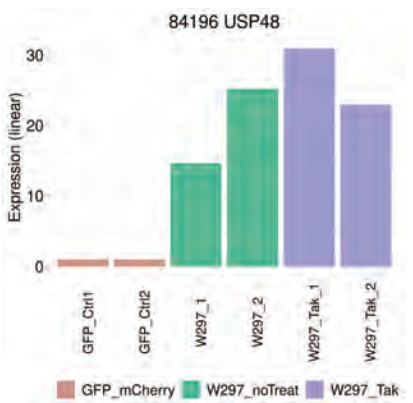

C

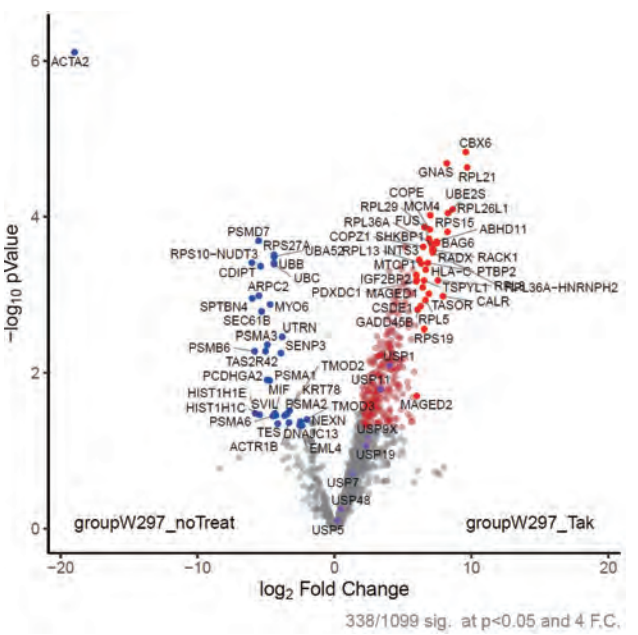

S3

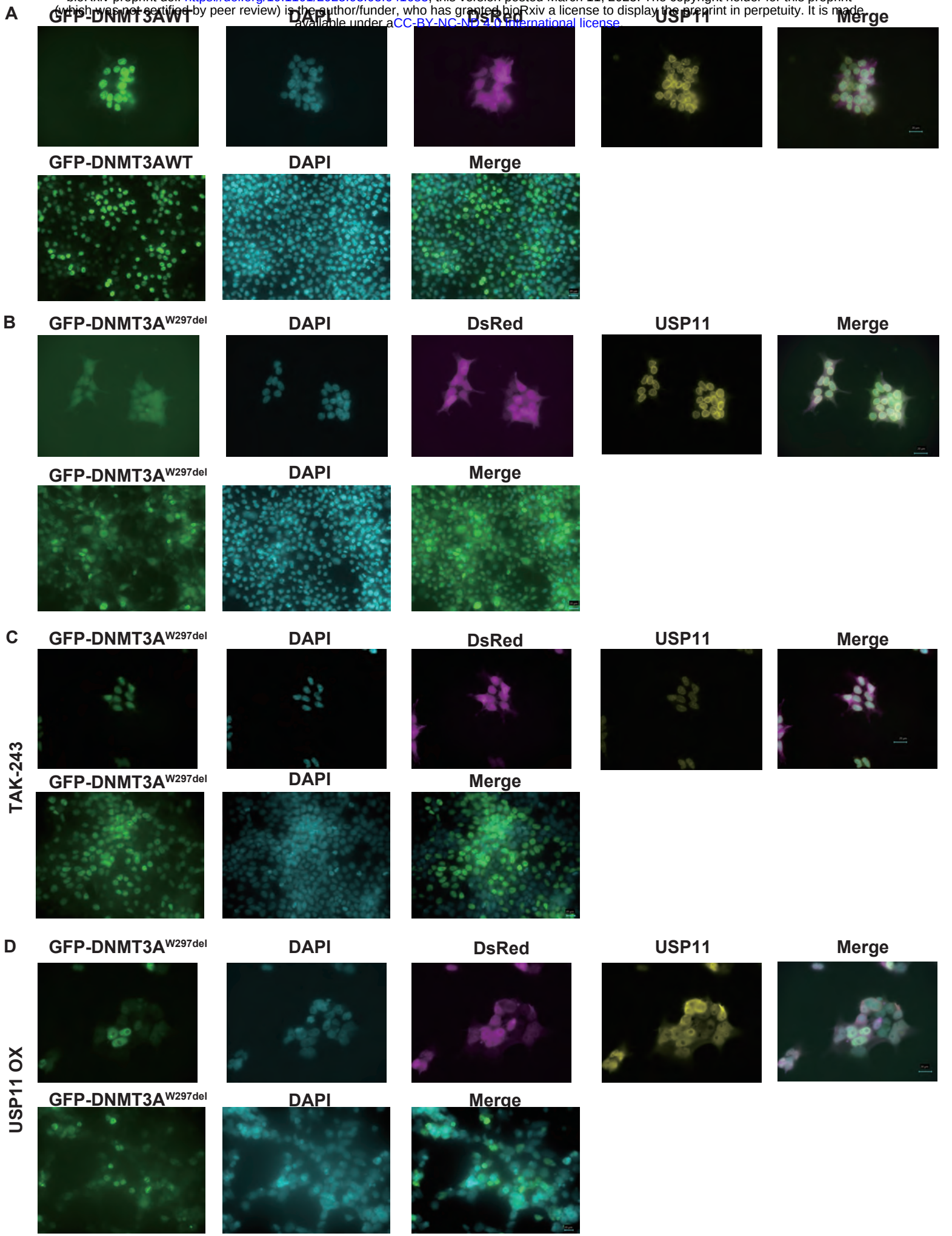

A

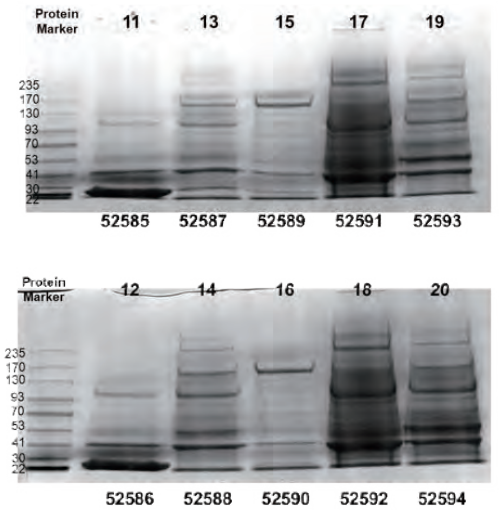

Well no.	Tube Label
11	GFP-Dsred-1(Negative control)
12	GFP-Dsred-2(Negative control)
13	GFP-DNMT3A1 Dsred-1
14	GFP-DNMT3A1 Dsred-2
15	GFP-DNMT3A1Dsred-1 DCAF8 KO
16	GFP-DNMT3A1Dsred-2 DCAF8 KO
17	GFP-DNMT3A1 297 del mt-Dsred-1
18	GFP-DNMT3A1 297 del mt-Dsred-2
19	GFP-DNMT3A1 297 del mt-Dsred-1 DCAF8 KO
20	GFP-DNMT3A1 297 del mt-Dsred-2 DCAF8 KO

B

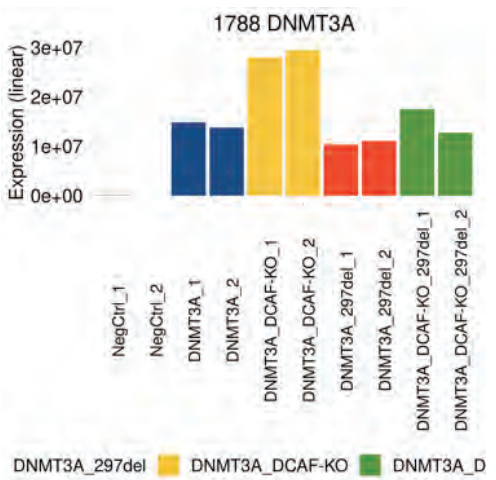

C

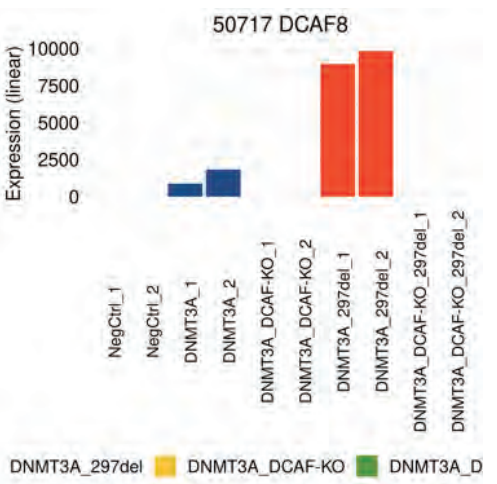

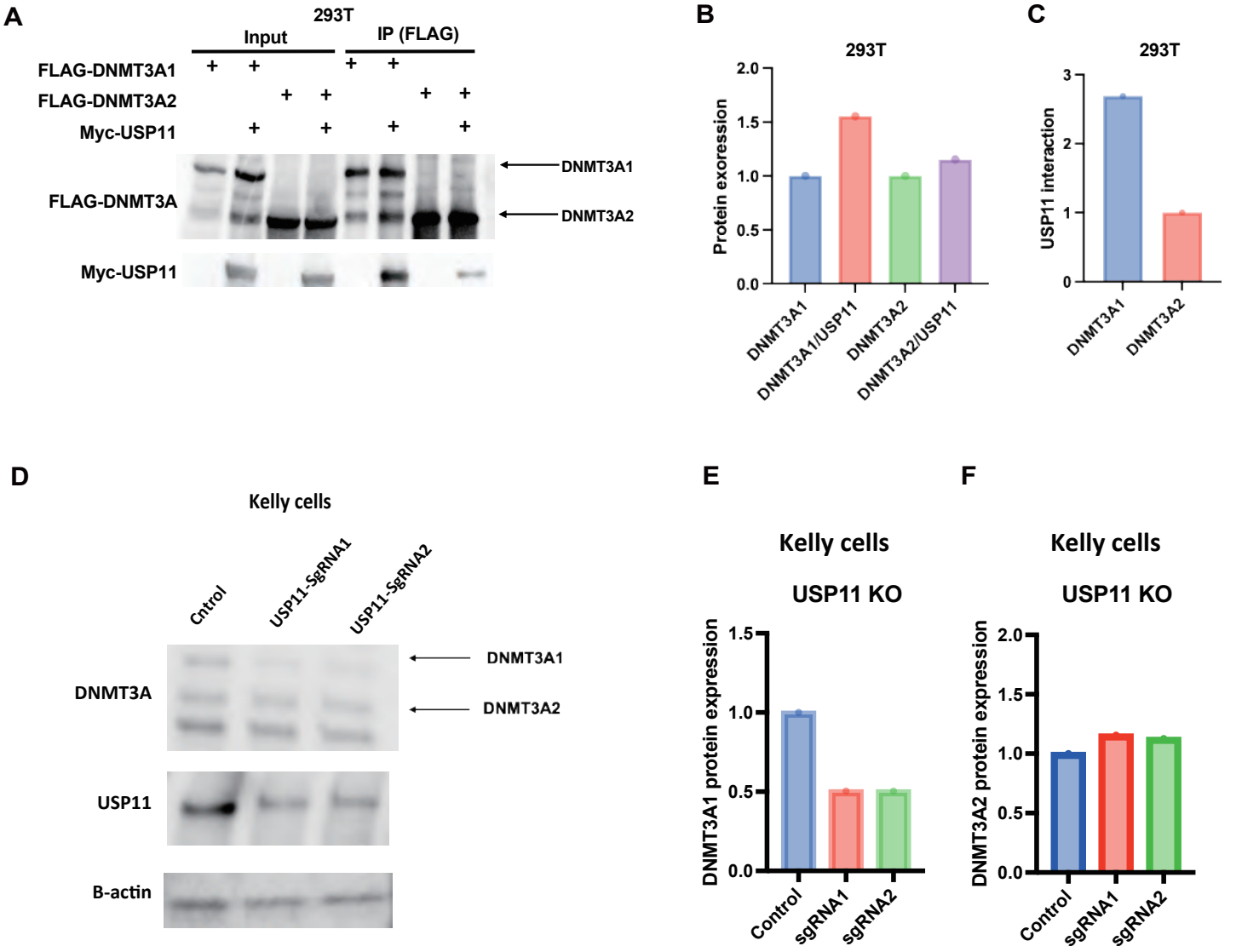

A

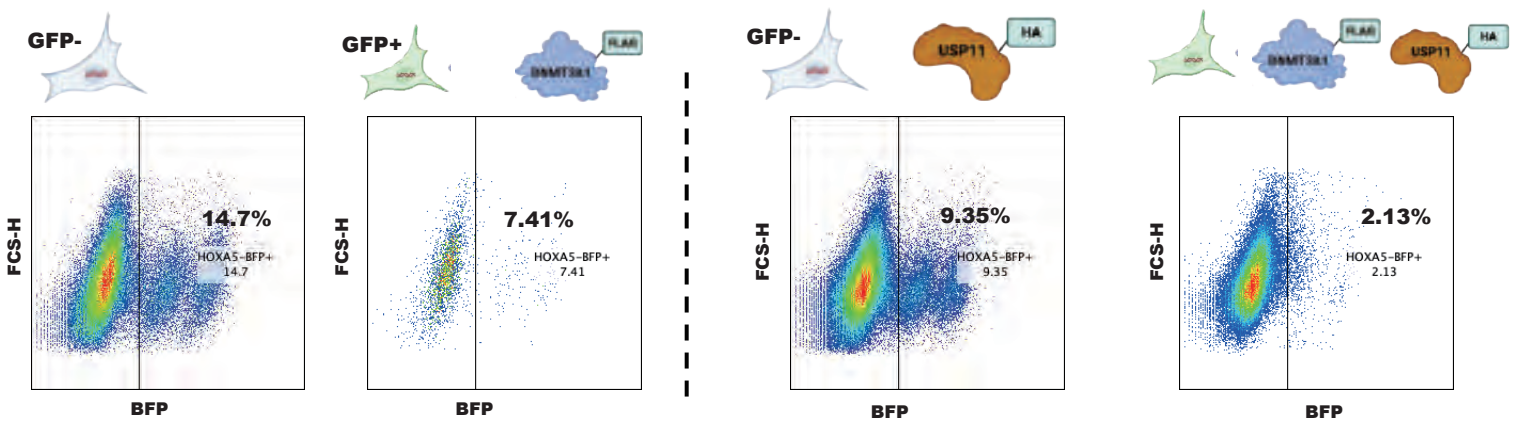

B